Physical Oceanography of the Persian Gulf, Strait of Hormuz, and the Gulf of Oman — Results from the *Mt. Mitchell* Expedition

R. Michael Reynolds
Brookhaven National Laboratory
Upton NY 11973 USA

August 1993

Abstract

The NOAA research vessel *Mt. Mitchell* operated in the ROPME Sea Area (RSA), comprised of the Persian Gulf, Strait of Hormuz, and Gulf of Oman, from February to June, 1992. Of seven separate legs, six official legs and one unofficial leg on the homeward journey, four were devoted primarily to physical oceanographic measurements. Basin-wide surveys of bottom sediments and biological variables were also undertaken but those results are not covered here. A variety of physical oceanographic observations were taken: (1) over 500 CTD casts were made; (2) seven current meter moorings were deployed and six were recovered yielding eleven, quality current meter records at different depths; (3) thirty-six drifting buoys with Argos positioning were deployed; and (4) continuous shipboard measurements of meteorological and oceanographic variables were recorded. The expedition data base continues to grow as new data from coastal meteorological and tide stations are added. The measurements are reviewed from the experimental point of view. Data accuracy, resolution, and precision are discussed and quality assurance of the measurements is reviewed. The complete data set covers the important seasonal transition from mid-winter to early summer. During this period of time, solar heating created an intense thermocline which decoupled the surface mixed layer from the interior water. The data are reviewed in the light of prior measurements and recent modeling results.

August 1993 — Submitted to the Marine Pollution Bulletin*, Pergamon Press, London.*

1 Introduction

The oceanic region comprised of the Persian Gulf (also known as the Arabian Gulf or simply the Gulf), Strait of Hormuz, and Gulf of Oman (Fig. 1) is one of the most important waterways in the world. In peak periods, one ship passes the Strait of Hormuz each six minutes (Al-Hajri, 1990), and approximately 60% of the world's marine transport of oil comes from this region. Surprisingly, then, the number of direct oceanographic observations from this region is small. Investigations have been undertaken by individual countries in their coastal waters, but only two basin-wide studies are commonly cited. Emery (1956) reported on a 1948 summer cruise by the German ship *Meteor*, and Brewer and Dyrssen (1985) reported on the 1976, wintertime expedition of the *Atlantis* from Woods Hole Oceanographic Institution. The primary reason for the dearth of basin-wide data is that political unrest between the countries bordering the RSA prevents scientific access.

The deliberate discharge by Iraqi soldiers of 6.3 million barrels (Mbbl) of crude oil during the 1991 war against Kuwait was an extreme act of environmental terrorism (Williams, 1991; Congressional Research Service, 1992). From 19–28 January, 1991, oil poured from two major sources (Fig. 2): three Iraqi tankers anchored at Kuwait's port of Mina Al-Ahmadi, and the Mina Al-Ahmadi Sea Island terminal area. The valves at the Al-Ahmadi terminal, 16 km offshore, were opened on 22 January, 1991, and were left open for four days until U.S. Air Force precision bombs partially closed the manifold. Five other tankers and several other terminals added more oil throughout the spring and early summer. Estimates of the oil spilled at Al-Ahmadi were based on duration and typical flow rates, and as such are approximate. An additional 0.28 Mbbls were spilled at Kafji and 0.19 Mbbls were spilled at Mina Bakr.

This spill was the largest oil spill in history. It was about twice the size of the next largest spill, Ixtoc, but on a more concentrated time and space scale. The third largest spill, also in the Gulf, occurred in the Nowruz field during the Iran-Iraqi war. The Nowruz spill came to 2–4 Mbbls, and was also an Iraqi creation.

An international program to study the effects of the oil spill on the environment began later in 1991. The program was sponsored jointly by ROPME, the Intergovernmental Oceanographic Commission (IOC), and the National Oceanic and Atmospheric Administration (NOAA). NOAA provided the research vessel *Mt. Mitchell*, which operated in the RSA from February to June, 1992. The expedition has been named the "*Mt. Mitchell* Expedition." All ROPME countries, with the exception of Iraq, supported the cruise and gave permission for the *Mt. Mitchell* or its small boats to enter into all coastal waters.

Essential studies of the environmental consequences of the war were planned. In addition, the cruise was seen as an important opportunity to make a comprehensive physical oceanographic study of the entire region. An ambitious program was designed, and the required instrumentation had to be procured, prepared, and loaded onto the ship during a scant three months before its sailing date on 15 January 1992: (a) several scientific vans were placed on the already limited deck area; (b) new instrumentation was purchased or upgraded including five new CTD units, a scientific-grade weather station, and an underway thermosalinograph; (c) two rigid hull inflatable boats (RHIBs) were bought and outfitted with lights, radios, and redundant navigation equipment; (d) a complete scientific shipboard computer (SCS) system was installed so all ship measurements and navigation could be monitored continuously; (e) below deck adjustments to living areas were made to accommodate the large complement of scientists; and (f) a personal computer network was installed and interfaced with the ship's Vax-based system. The ship crew

graciously made way for an anticipated scientific party of up to 22 which changed on each leg.

The cruise lasted from 26 February to 12 June, 1992 (Julian days 57-160) during seven at-sea periods (Table 1). The cruise final report (National Oceanographic and Atmospheric Administration, 1993) provides an excellent overview of all the various activities. Figures 1 and 5 show the approximate locations of the different physical oceanographic measurements made from the *Mt. Mitchell* and Table 2 lists the most important measurements. The *Mt. Mitchell* study was necessarily broad, only touching on several areas of interest and lighting the way for future detailed investigations.

This paper reviews only the basin-wide physical oceanographic measurements taken during Legs I and VI. Leg III, an intensive hydrographic survey of the Iranian coastal waters (see Galt, 1993), is beyond the scope of this paper. Iranian coastal flow is an important feature in the circulation patterns and is easily seen in the satellite images and shuttle photos.

2 Background

Geographic Features

The Persian Gulf is separated from the Gulf of Oman by the Strait of Hormuz, which is only 56 km wide at its narrowest point. There is no sill in the Strait of Hormuz; the trough simply deepens to more than 100 m through the Strait and drops quickly to more than 2000 m within 200 km outside the Strait. The maximum width of the Persian Gulf is 338 km, and the length to its northern coast is nominally 1000 km. The surface area of the Gulf is approximately 2.39×10^5 km^2, and a mean depth of 36 m implies an average volume of 8.63×10^3 km^3.

The bathymetry of the Persian Gulf (Fig. 1) shallows to the northwest and to the west coasts. An isolated trough extends northward from the Strait of Hormuz along the Iranian coast approximately 100 km. The trough collects denser bottom water and impedes exiting bottom flow. The possibility exists that a weak bottom circulation into these depressions could lead to a build-up of pollutants. Fine grained muds are found in this area, which supports the theory (Hughes and Hunter, 1979; Reynolds, 1992a) .

The broad region of shallow water off the coast of the United Arab Emerites (UAE) features many small islands and lagoons where it is extremely difficult to operate oceanographic vessels. This area is a region of intense evaporation, and a significant contribution to the deep circulation of the Gulf is made here. (Unfortunately, the *Mt. Mitchell* was unable to make measurements here.)

Fresh Water Exchange

Evaporation in the Persian Gulf is much higher than both river inflow and precipitation and the net loss of water creates a Mediterranean, reverse-flow, estuarine circulation. Estimates of evaporation vary from 500 cm yr^{-1} to 144 cm yr^{-1}. The lower figure from Privett (1959) is in agreement with Meshal and Hassan (1986) who estimated 200 cm yr^{-1}, and this latter term is probably closer to the actual amount. Measurements indicate that even though the water temperature is considerably higher in the summer, most evaporation occurs in the wintertime, due mainly to the higher wind speeds.

Most river inflow into the Persian Gulf occurs in the northern end, primarily on the Iranian side (Fig. 2). Recent river volume flow measurements were provided to the *Mt. Mitchell* scientists

by Iranian participants. The new data allow a better estimate of outflow than has hitherto been available. The Shatt Al-Arab is a nexus of three major rivers: the Tigris and Euphrates rivers together provide an annual average of 708 $m^3 s^{-1}$ and the Karun adds 748 $m^3 s^{-1}$. Thus, the total average outflow of the Shatt Al-Arab is 1456 $m^3 s^{-1}$. Other major rivers are the Hendijan (203 $m^3 s^{-1}$), the Hilleh (444 $m^3 s^{-1}$), and the Mand (1387 $m^3 s^{-1}$).

The total river runoff is 1.1×10^2 $km^3 yr^{-1}$, equivalent to 46 $cm\,yr^{-1}$ of depth. This estimate, from Iranian river measurement reports, is considerably greater than earlier published estimates and needs further verification. Al-Hajri (1990) uses a value of 16 cm yr^{-1}. Industrial and agricultural development are having a pronounced effect on the outflow from the Shatt Al-Arab, where annual runoff has decreased substantially over the past twenty years.

Annual rainfall in the arid climate of the RSA is small, of the order of 7 cm yr^{-1}. Rainfall makes a negligible contribution to the fresh-water budget of the RSA.

Winds

The RSA is located between latitudes 24–30°N in which are located most of the Earth's deserts. This region marks the boundary between tropical circulations (Hadley Cell) and the synoptic weather systems of mid-latitudes. Descending dry air in these latitudes produces clear skies and arid conditions.

In the north, the local climate is influenced by orography. The Taurus and Pontic mountains of Turkey, the Caucasus mountains of Iran, and the Hejaz mountains of the Arabian Peninsula together with the Tigris-Euphrates Valley, form a northwest-southeast axis that strongly influences the tracks of extra-tropical storms to a southeast direction.

The climate in the Gulf of Oman is markedly different than the climate in the Persian Gulf. While the Persian Gulf is affected mainly by the extra-tropical weather systems from the northwest, the Gulf of Oman is at the northern edge of the tropical weather systems in the Arabian Sea and Indian Ocean. This monsoon circulation produces southerly winds in the summer and strong northerlies in the winter. The Strait of Hormuz approximates a boundary between the two systems.

The most well-known, and notorious, weather phenomenon in the Persian Gulf is the Shamal, a NW wind which occurs year round (Perrone, 1981). Shamal is an Arabic word meaning north. The Winter Shamal is a wind that sets in with great abruptness and force, and is related to synoptic weather systems to the NW. It seldom exceeds 10 $m\,s^{-1}$ ($< 5\%$ frequency) but lasts several days. The summer Shamal is practically continuous from early June through July. It is associated with the relative strengths of the Indian and Arabian thermal lows.

The winter Shamal brings some of the strongest winds and highest seas of the season to the RSA region. Winds in the area ahead of an approaching cold front blow from the southwest. These winds, called *Kaus* in Arabic or *Shakki* in Persian, slowly increase in intensity as the front approaches. They may reach gale force before the passage of the front and the onset of the Shamal. Due to the channeling of the low-level air flow by the Zagros mountains of western Iran, the strongest of the southerly winds occur on the eastern seaboard. The Shamal usually occurs first in the northwest and then spreads south.

A strong sea breeze occurs along the entire coastline, especially along the Arabian peninsula. Driven by the intense temperature difference between the land and water surfaces, the sea breeze circulation adds a landward component to all winds. The effect of these winds is to drive surface pollutants (oil and others) to the beach much faster than they would move otherwise. Examples

of on- or off-shore winds as high as 15 $\mathrm{m\,s^{-1}}$ are evident in coastal meteorological stations.

Currents – tides, wind-driven, and density-driven

The energy in the water motion can be related to three forcing processes: tidal forces, wind forces, and density differences. The kinetic energy of the water velocity can be partitioned among the three terms approximately as 100, 10, 1 respectively. Each of the different currents has a different scaling time: tides vary over a few hours at diurnal or semidiurnal periods; wind-driven currents develop and subside over a few days; and density-driven currents take weeks to change in response to seasonal forcing. These three current components can be extracted from measurements, but the selection of averaging times and filter types affects the computed proportions considerably and must be used with care. Because of their consistent direction, density currents are important in the distribution and removal of pollutants from the RSA region. Hence, considerable attention is paid to these features.

Tides

The tides in the Persian Gulf co-oscillate with those in the narrow Strait of Hormuz, which opens into the deep Gulf of Oman (Fig. 3). The tides in the Gulf of Oman co-oscillate with those in the Arabian Sea. The tides in the Persian Gulf are complex standing waves and the dominant pattern varys from being primarily semi-diurnal to diurnal. The tidal range is large, with values greater than 1 m everywhere (Lehr, 1984). The dimensions of the Persian Gulf are such that resonance amplification of the tides can occur and the result is that the semi-diurnal constituents have two amphidromic points, in the northwest and southeast ends, and the diurnal constituents have a single amphidromic point in the center near Bahrain.

Tides are important for stirring and mixing waters vertically and on a horizontal scale of 10 km, but they do not make an important contribution to the residual circulation of the RSA. Tidal current averages longer than a day have negligible residual energy, and as a result, basin-scale advection from tides is not considered by oil trajectory models or general circulation models. Tides are important on smaller scales of horizontal length (< 10 km) and time (< 24 hrs).

Residual Circulation – wind-driven and density-driven

The main features of the residual circulation in the Persian Gulf are (Hunter, 1983): (a) high- and low-salinity water exchange in the Strait of Hormuz; (b) density-dominated circulation in the central and southern regions; (c) frictional-balanced, wind-dominated circulation in the NW region; and (d) evaporation-induced bottom flow. The actual pattern of circulation is complex, as can be seen by the patterns of sea-surface temperature shown in Fig. 4.

Water exchange with the Gulf of Oman dominates the circulation of the southern Persian Gulf. The net freshwater loss to the atmosphere is replaced by a surface inflow in the Strait of Hormuz. Throughout the year and against prevailing Shamal winds, relatively low-salinity water enters through the Strait of Hormuz to freshen the hypersaline water. High evaporation increases the density of the surface water so that it sinks to exit as a high-salinity undercurrent through the deeper portion of the Strait of Hormuz. This reverse estuary flow is similar to the circulation of the Mediterranean Sea.

An important, secondary current in the Persian Gulf is a coastal, reverse circulation along the Iranian coast. Driven by the density differences that result from river runoff, the coastal currents along the Iranian coast are southerly, against the inflow water. The reverse currents are evident in shuttle photographs and AVHRR images (Fig. 4). The interface between the two

currents is a region of horizontal current shear which often shows evidence of wavelike shear instability.

Circulation in the Gulf of Oman includes the following features: (a) outflow at depth from the Strait of Hormuz sinks to a depth of approximately 200 m and spreads across the basin and (b) counter-rotating gyres which create a cold-water, upwelling feature along the Iranian coast. The Gulf of Oman is a transition from estuarine to deep-ocean circulations.

Mixing Processes and Vertical Structure
There are three, primary contributors to mixing of the water column: (1) tides, (2) winds and waves, and (3) evaporation. Internal waves at density interfaces, and topographic features such as island also contribute to mixing, but their contribution is unknown and probably small. The strong tidal currents create a bottom, mechanical, turbulent friction layer. The enhanced turbulent mixing homogenizes the water column from the bottom up, and a bottom mixed layer is evident in all hydrographic sections. The other two mechanical mixing processes are strongest at the surface. Wind friction creates a surface shear layer and also creates surface wave fields, both of which form a surface mixed layer. Evaporation of fresh water enhances mixing by increaseing the salinity and density of the surface water, thus reducing surface stability. In the winter, combined cooling and evaporation increase the density sufficiently to overturn the water column and, north of Qatar, create a well-mixed water column.

Mixing processes are opposed by the stabilizing effects of surface warming. As the temperature increases, the water density decreases. Countering this stabilization, evaporation increases surface salinity, which increases density and creates an unstable overturn to some lower depth. The resulting surface mixed layer and lower thermocline reach about 20 m depth (Fig. 12). The density contours (σ_T) indicate the combined effect of temperature and salinity.

Residence Times

The estuarine circulation exchanges water between the Persian Gulf and the Gulf of Oman via the Strait of Hormuz. Simple box models predict the residence time for a water parcel in the Gulf. (Assuming a long-term steady state and instantaneous, perfect mixing, the residence time is the ratio of volume of water to the volume exchange rate (in or out) of the Gulf. It is a measure of the mean amount of time a parcel of water will remain in the volume. We assume the same measure applies to passive pollutants.) Up to now, the circulation in and out of the Strait of Hormuz has been poorly defined, and as a result estimates of residence times vary in the approximate range of 2-5 years (Hughes and Hunter, 1979; Hunter, 1983). However, knowledge of the circulation in the Strait of Hormuz plays a key role in understanding the basin-wide behavior of the Gulf.

Thus a parcel of water in the northern end of the Persian Gulf may have a much larger residence time than one in the southern end. We have noted the distinct difference between the northern and southern ends. The north is shallow and dominated by wind friction. River outflow at the north end plays a role in the local circulation there. At approximately the longitude of the Qatar peninsula, density-driven, negative-estuary conditions prevail. High evaporation in the broad coastal areas on the coast of UAE provide much of the saline bottom water that feeds the bottom outflow through the Strait of Hormuz. These differences are yet to be fully investigated, but the information from the *Mt. Mitchell* Expedition will provide data to make these assessments.

Surface Pollutant Trajectories

Water at the ocean surface is strongly influenced by the winds over the water. A rule of thumb is that the wind-induced surface flow is 3% of the mean wind speed and 15° to the right of the wind direction (northern hemisphere). In a 10 $\mathrm{m\,s^{-1}}$ Shamal wind this amounts to an 0.3 $\mathrm{m\,s^{-1}}$ added current, which is larger than expected residual currents (approximately 0.1 $\mathrm{m\,s^{-1}}$). Over several tidal periods, knowledge of wind-induced surface currents plays a significant role in predicting surface pollutant trajectories.

In an enclosed basin such as the Persian Gulf, sustained winds such as Shamals generate secondary circulations over the entire basin. The secondary flow gyres oppose and even nullify residual, wind-induced currents in some regions. An example of this effect is the very low observed drift over several months of the drifting buoys in the central northern gulf (discussed below).

Modeling Studies

Probably no other body of water of comparable size and economic importance is so underinvestigated as the RSA. Modeling efforts have been carried as far as they can with the present, spotty data base. Winds and hydrography and the resulting currents are highly seasonal, and a lack of data sets for all seasons adds another dimension to the problem. An extensive modeling effort is one means of bridging the data gap.

Modeling efforts can be divided between tidal models and estuarine circulation models. Three comprehensive models of the estuarine circulation currently exist: (1) The U.S. Naval Oceanographic Office (Horton, et al., 1992); (2) The Catholic University of America (Chao et al., 1992); and (3) King Faud University of Petroleum and Minerals (KFUPM) (Lardner et al., 1987; Lardner et al., 1988a; Lardner et al., 1988b; Lardner et al., 1991; and Lardner et al., 1993). The Navy model is a three-dimensional, primitive-equation circulation model with complete thermodynamics and imbedded turbulent-closure submodels. It uses terrain-following vertical coordinates and has a horizontal grid size of approximately 8 km and 14–22 levels in the vertical. The Catholic University model uses 20 km grid size and 11 levels in a diagnostic formulation. The KFUPM model covers the gulf with a rectangular grid of approximately 10 km size. It is three-dimensional, but has the option of being run in a two-dimensional, vertically-integrated mode. The algorithm uses a mode-splitting method by which the depth-averaged equations are first solved for the barotropic mode, then the momentum equations are stepped forward to compute the velocity profiles. The bottom friction and advective terms are computed for use in the depth-averaged equations on the next step. These models all produce similar large-scale patterns which are summarized in the conclusions below.

There are several excellent tidal models for the Persian Gulf, and the paper by Le Provost (1984) is a good review. As discussed in Sec. 2, tides are oscillatory and contribute little to the residual current flow. Thus, for scales beyond the tidal excursion (< 10 km), they contribute little to advection processes. They do contribute to horizontal and vertical mixing, mainly by production of mechanical turbulence over the sea bed and around obstacles. The KFUPM has developed a detailed tide model of the Gulf (Lardner et al., 1982).

Oil spill models have been developed for the Gulf. Galt (1983) and Galt et al. (1983) describe a finite-element circulation model developed during the Nowruz spill and subsequently updated for the recent spill.

3 Methods

Hydrography

Legs I, III, and VI were dedicated to physical oceanography, and conductivity-temperature-depth (CTD) measurements were a major part of them. Details of the methods used at sea can be found in Reynolds (1992a and 1992b). Standard hydrographic algorithms were used to compute salinity from conductivity, temperature and pressure. From salinity and temperature, the density, $\rho(T, C, p_0)$, is computed in the form of σ_t,. where $\sigma_t = \rho - 1000$ kg m^{-3} and p_0 is standard atmospheric pressure at sea level.

CTD casts were made from the ship and two Rigid Hull Inflatable Boats (RHIBs). To meet the expected requirements and provide backup, two Seabird Electronics Company, SBE-9, real-time, shipboard CTDs and three SBE-19 Seacat internally recording CTDs were provided. Because of an early requirement for dissolved oxygen (DO) profiles concurrent with the CTD casts, one SBE-9 and one SBE-19 had DO sensors. The requirement for DO measurements was later removed, and although DO profiles were made at many stations, the DO sensors were not calibrated or maintained during the cruise. Post calibrations of the sensors showed that all sensors, including DO, were within specified accuracy limits at the end of the cruise. The SBE-9 CTD was housed in a protective cage and installed in a General Oceanics rosette sampler configured to accept 12, 1.7 l, Niskin bottles.

Making more than 112 CTD stations throughout the RSA in less than two weeks, along with other project activities, was a stringent requirement, and the RHIBs were designed for this goal. The two 17-foot RHIBs were outfitted with 100 hp outboard motors, fathometers, HF and VHF radios, hand-held GPS and LORAN-C navigation receivers, and extra fuel tanks carrying a total of 54 gallons of gasoline. In calm seas they could travel at 30 kts for periods of up to six hours. Each RHIB was fitted with a small electric winch with 123 m of 60-kg test-tensile-strength, stainless steel wire to aid in the deployment and recovery of the CTD units.

Quality Assurance of the CTD measurements was maintained by several methods: (a) Intercomparison casts were taken with at least one Seacat attached to the rosette frame. In general, temperature and salinity intercompared to ± 0.02 (°C or psu, respectively). (b) Intercomparison soakings of several units were regularly made. (c) Rosette water samples were taken from 23 different stations during the legs. The general performance of the equipment was good, but the quality of the soundings noticeably declined over the duration of the cruise. Most importantly, strong temperature and salinity gradients produced spiking in the computed salinity and σ_t profiles. Strong gradients in temperature or salinity are known to induce spiking as a result of differing time constants in the temperature and conductivity sensors. All casts are currently undergoing a spiking removal analysis.

Current Meter Moorings

Current-meter moorings were deployed with the objectives of (a) better understanding the circulation in the central Persian Gulf, (b) monitoring the variation of the two-layer estuarine exchange with the Strait of Hormuz and Gulf of Oman, and (c) denoting the extent of the surface inflow water from the Strait of Hormuz along the Iranian coast. The mooring locations (Fig. 5) were compromises based on ship traffic patterns, political and industrial boundaries, and scientific objectives. Five anchored moorings (Fig. 6) were provided by the NOAA Pacific Marine Environmental Laboratory (PMEL). With the benefit of equipment loaned by the University

of Qatar, two additional moorings were deployed. Of the seven moorings and sixteen current meters deployed, five moorings with eleven operating meters were recovered. Mooring M6 was lost due to failure of some of the flotation spheres, possibly from collision with a deep-draft ship. Mooring M1 was never found and it is suspected it fell victim to the heavy bottom-trawl fishing in the southern Gulf. Finally, the top meter of mooring M7 failed to advance its tape. Table 3 is a summary of the recovered current-meter time series.

All current meters were Aanderaa Model RCM-5 with magnetic tape recording. The meters measured current speed by counting rotations of a savonius rotor, current direction by recording a magnetic compass bearing, temperature from a thermistor resistance bridge, conductivity by an inductive sensor, and pressure from a capacitive sensor. All measurements except speed were taken once at the end of the speed counting period, which for this experiment was set to 20 minutes. The accuracy of the speed, direction, temperature, condutivity, and pressure are estimated to be 1 $\mathrm{cm\,s^{-1}}$, 2°, 0.1°C, 0.01 $\mathrm{S\,m^{-1}}$, and 1 dbar, respectively. The corresponding recorded resolutions are 1 $\mathrm{cm\,s^{-1}}$, 1°, 0.1°C, 0.01 $\mathrm{S\,m^{-1}}$, and 0.1 dbar. The accuracy and resolution of the computed salinity is 0.1 psu and 0.01 psu, respectively.

With the exception of conductivity, measurement quality was good throughout the deployment period. Algal growth developed on all meters during the three-month deployment, with the densest growth on near-surface meters. Within a few weeks of deployment all conductivity measurements became questionable. From initial inspection of the data, it is felt that in no case was the savonious rotor impeded by algae and that the speed measurements did not deteriorate over the deployment time. All NOAA meters were post-calibrated immediately after the ship returned to the USA and were found to be within specifications.

Preliminary analysis of the current meter data was performed using the Matlab statistical software programs. Residual currents were estimated by use of a low pass filter designed by the Woods Hole Oceanographic Institution (WHOI), the PL133 low-pass filter (Flagg, et al., 1976). The PL133 is a sharp-cutoff, symmetric, convolution window with 65 elements in the time domain. All frequencies from 0–0.02 $\mathrm{hr^{-1}}$ (DC to 2 day period) are passed with negligible attenuation. The 10-db cutoff frequency is equal to the O_1 tide frequency of 0.04 $\mathrm{hr^{-1}}$. The filter represents a compromise that suppresses most tidal fluctuation, yet passes short period wind induced fluctuations with periods of a few days. The filtered data exhibit some oscillations of near-diurnal period that may be a leaked tidal signal or internal waves with frequencies below the filter cutoff.

Drifting Buoys

Thirty-two Argos-tracked drifting buoys were deployed in the *Mt. Mitchell* study (Table 4). Five different types of buoys were used (Fig. 7) (a) Davis Design: based on a special design by Davis (1985a, 1985b), this buoy had negligible error from wind drift and wave rectification. It is considered to be the most accurate buoy for surface current measurements. (b) CMOD: air-deployable design manufactured by the Metocean Company. When this compact buoy entered salt water a spherical float inflated, the antenna telescoped up, and a holey-sock drogue droped to eight meters. (c) ECOCAP type: a large FGGE-style buoy manufactured by the French agency CEIS ESPACE. This buoy incorporated an 0.5 m, square window shade drogue centered at approximately 3 m. (d) Low cost drifter (LCD): a very small buoy that had no drogue and was specially weighted in hopes it would properly represent the drift of an oil slick. (e) Spherical surface drifter (SSD): a small spherical-shaped buoy also with the purpose of simulating oil slicks.

The Davis drifter buoy provided exceptionally accurate current following in the presence

of wind and surface waves. The hull design minimized non-linear rectification of drag forces induced by short-wave motion so that the mean drag averaged to near zero over a complete wave cycle. Wind drag was also minimal since the antenna was the only thing exposed above the water. Tests by Davis (1985a) verified that design goals were achieved. The buoy motion agreed with the water motion at a depth of approximately 0.5 m, and typical slip velocity was less than 1 $\mathrm{cm\,s^{-1}}$ and never exceeded 1.5 $\mathrm{cm\,s^{-1}}$. Brightwaters Instrument Co., Brightwaters NY manufactured the Davis drifters in an economical package so that a large number could be deployed to provide complete coverage of the RSA.

Six Compact Meteorological and Oceanographic Drifter (CMOD) buoys were provided by the U.S. Navy. The sonobuoy-size CMOD buoys were self-contained units designed for three to four months operation. The buoys were 0.123 m dia×0.917 m long, and weighed 12.7 kg. The flotation was an inflatable collar and the antenna was a two-part telescopic mast. The drogue was an 8-m holey sock drogue resulting in a center of drag at approximately 4 m depth. On three occasions, CMOD buoys were released concurrently with Davis buoys for intercomparison purposes.

Four ECOCAP buoys were donated to the program by the Marine Environmental Protection Agency (MEPA) of Saudi Arabia (Tawfiq, 1987). The buoys were large cylindrical buoys, approximately 0.3 m dia. × 2 m long. A one-meter piece of chain and a 0.5×0.5 m window-shade drogue were suspended beneath the buoy. The combination cylinder, chain, and window shade resulted in a center of drag at about two meters.

Two oil-spill buoys were provided by the U.S. Minerals Management Service (MMS). Oil-spill buoys are designed to have the right combination of wind and water drag so they will drift in the same direction as an oil spill. These buoys are small, have no drogue, and are designed to operate only a few days while they are in the vicinity of the spill. The Low-Cost Drifter (LCD), manufactured by Aanderaa Instruments Co. based on a design from Draper Labs, was a discus-shaped buoy approximately 0.5 m dia. The Spherical Surface Drifter, (SSD), an experimental design, is approximately the same volume as the LCD, but is spherical and depends on a one-kg fishing weight to keep it upright.

Buoy location was computed by CLS/Argos from telemetry to the NOAA polar-orbiting satellites (Argos User Manual, 1988) . Location and buoy measurements, such as sea-surface bulk temperature, were transferred automatically from CLS/Argos to the NOAA/PMEL computer by FTP (file transfer protocol) over the Internet. The Argos User Manual estimated the number of daily passes over a platform at the latitude of the Gulf (30°N) to be 8–12 with a mean of 9. The time window during which the satellite was in view and could receive messages had an average duration of ten minutes. The buoys transmitted one-second beacons at a 90-second period. Latitude and longitude computations have RMS errors of 200 m and 600 m, respectively. Over the course of the experiment, the mean arrival time between consecutive location fixes was 2.2 hours (10.9 positions per day) but there were some gaps of as much as 12 hours, and these are expected to complicate detailed analysis because of the aliased tidal signal.

Each buoy data set was edited, smoothed, and interpolated onto a common time base. Missing data blocks and any other errors were corrected as they occurred. The time series were interpolated to a common three-hour time base ($0, 3, 6 \ldots, 21$ UCT) with a cubic-fit interpolation routine which preserved the original position and velocity information at each measured point and had much less overshoot than standard cubic spline techniques. Each buoy record was examined carefully, and only free-drift data were retained for further analysis. The drifting buoys suffered a variety of fates: some ran aground, some were picked up by fishing boats, and

some ceased transmitting without reason.

Support from Space

To supplement the field surveys and to serve as an aid to data interpretation, astronauts aboard the Space Shuttle *Atlantis* photographed water features and coastal habitats in the Gulf during mission STS-45 from 24 March to 2 April, 1992 (Ackleson et al., 1992). The astronauts collected 111 hand-held, color photographs from an altitude of 296 km. The photographs were an important tool because they provided visual support to the picture surmised from measurements. Of special interest were the distributions of turbidity which resulted from river outflows and from the Iranian coastal currents.

The NOAA series of polar-orbiting satellites collected images of sea-surface long-wave radiation with its Advanced Very-High Resolution Radiometer (AVHRR) instruments. The one-km-resolution images were collected by NASA as part of their overall support of the expedition. By using a telephone link via Inmarsat-A, NASA was able to send thermal images directly to the ship within a few hours of their collection. The images were used to fine tune daily activities and as confirmation of the observed measurements.

4 Results

Meteorology. The winter of 1991-92 was one of the coldest ever registered in that area of the world. In February it snowed in Israel and Lebanon for the first time in most people's memory, and Turkey recorded extensive cold and snow. The temperature in the western Middle East had a strong effect on the RSA. The winter temperatures in the northern RSA were 4–5°C colder than normal, reaching almost 14°C in the far north. These low temperatures were suspected to be a reason for extensive coral devastation in this region.

Processed meteorological data from the Shipboard Computer System (SCS) provided an interesting overview of over-the-water conditions related to evaporation. An example of the air and water temperatures and the true wind speed is given in Figure 8. During winter and early spring (days 57–100), the air-sea temperature difference was negative (air colder than the water) which created an unstable and convective boundary layer with enhanced evaporation. As summer approached (after day 110 approximately), the air became warmer than the water which stabilized the surface layer. It is believed that most evaporation occurs in the wintertime as a result of the combined effect of higher winds and enhanced convection, though this is not yet fully substantiated. Summertime evaporation is enhanced by the buoyancy production from the very high humidity values over the water.

The cases of Shamal-type winds were numerous during the cruise. High winds (> 30 kts) were reported on the ship five times between days 57-137. On many occasions winds exceeded 40 $\mathrm{m\,s^{-1}}$ and the duration of the wind outbreaks generally lasted from two to several days.

Hydrography Figures 9 to 12 indicate that the surface inflow into the Gulf occurs year round, but is more pronounced and extends deeper in the summer. However, in the winter (Fig. 11) the density difference is primarily due to the lower salinity of the water of the Gulf of Oman where in summer (Fig. 12) both temperature and salinity strengthen the density difference.

Wintertime cross sections at A and C (Fig. 13 and Fig. 14) indicate how the bottom water exits the Strait of Hormuz. In Section C, very dense water ($\sigma_T > 27$) fills the bottom and

banks slightly upwards towards Oman. This water spills down the open mouth of the Strait of Hormuz, mixes with Gulf of Oman water, and ultimately settles out as a density layer at about 200 m ($\sigma_T \approx 26$). The bottom layer is stratified, and at the bottom temperature and salinity are 20°C and 40 psu, respectively. The slope of the isopycnals in the bottom layer is upwards toward Iran, which produces a geostrophic current component into Gulf. This direction does not agree with the negative-estuary model and gives some evidence that the outflow is seasonal.

Figures 11 and 15 show that the two-layer system of the southern Persian Gulf gives way to vertical mixing and becomes veretically mixed north of Section I. As shown by sections P (Fig. 16) and Q (Fig. 17), vertical mixing dominates stabilizing influences everywhere with one exception, the Shatt Al-Arab, fresh-water outflow which moves southward along the Kuwait coast.

Summertime cross-sections in the vicinity of the Strait of Hormuz reveal a similar picture of the water mass exchange. In section A (Fig. 18), the tongue of Gulf water at 200 m is apparent as a water mass with temperature of 20–21°C, salinity just above 37.5 psu, and a thickness of almost 200 m. In section C (Fig. 19), the stratified bottom layer is not evident. Instead, a 30-m-deep, bottom boundary layer of 20°C and 39.5 psu reflects the effects of tidal mixing. The sloping isopycnals of the bottom layer indicate an outflow. There is no doubt that the water exchange through the Strait of Hormuz is complex, and a detailed analysis of the *Mt. Mitchell* data is beyond the scope of this review.

The Section-I, summer cross-section is strongly stratified (Fig. 20). When this is compared with the well-mixed winter case (Fig. 15), we see evidence that the bottom water (*e.g.* 18°C and 40 psu) has crept downslope toward Iran. The water in the deeper areas cools and becomes more dense as the summer thermocline decouples the bottom water from the surface. The strength of the summer stratification is evident sections P and Q (Figs. 21 and 22). The thermocline depth here is approximately 18 m. At section Q, the vertical mixing is sufficient to eradicate the thermocline. The outflow of the Shatt Al-Arab, at a peak at this time of year, is pronounced along the Kuwaiti coast in these sections. The water at the bottom of section P is decoupled from the surface, but has warmed by about 5°C since winter. The data indicate that bottom water is created in the well-mixed cooled areas in the far north and then flows southward under the thermocline, forcing a southerly flow of bottom water over the entire Gulf region.

Mt. Mitchell data indicate the following features about the vertical structure of the RSA: (a) In the wintertime, north of Qatar, the water column is almost perfectly mixed top to bottom (Fig. 11). (b) In the summertime, the northern end of the Gulf becomes a two-layer system with a well-mixed surface layer and a well-mixed bottom layer which is a residual of the winter water (Fig. 12). (c) At the extreme northern end, the depth becomes shallow enough that surface and bottom mixing can stir the water column over its full depth. (d) At the southern end of the Gulf, the two-layer system persists year around. The upper layer of fresher water intruding from the Gulf of Oman replaces water lost by evaporation, and the lower, more-saline water exits to complete the the reverse-estuarine, Mediterranean-like circulation.

Current meters. Progressive vector diagrams (cumulative sums) of the filtered current vectors substantiate the density-driven, reverse-estuary circulation pattern (Fig. 23). The general pattern of inflowing surface current and outflowing bottom current can be seen in records from M2, M3, M4, and M7. Overall mean currents were in the neighborhood of 5 $\mathrm{cm\,s^{-1}}$. A weak, cross-basin flow of about 2 $\mathrm{cm\,s^{-1}}$ was evident in the records of M3, M4, and M5. The northward bottom current at M3 (71 m) is surprising and this record is currently being re-examined for

errors.

The temperature records (Fig. 24) reflect the estuarine circulation and the onset of the summer thermocline. Surprisingly, the bottom temperatures at M2, M3, and M4 actually *decreased* by approximately 1°C during the transition from winter to summer. The surface waters increased by about 7°C during this time period. The bottom cooling occured when the thermocline set up and the winter bottom water flowed southward, downhill into the deeper areas. The motion is apparent when comparing Figures 11 and 12.

Lagrangian drifter buoys. The primary objective of the drifting buoy program was to give a general overview of the circulation patterns in the Persian Gulf, Strait of Hormuz, and Gulf of Oman. Buoys were launched in various combinations (Fig. 5) for a variety of secondary goals: (a) buoy type intercomparisons, (b) dispersion and mixing estimates, and (c) circulations in a smaller space scale. Figure 25 provides an overview of the buoy behavior. There is indication of a clockwise gyre in the western Gulf of Oman with a counter-clockwise to the east. Sadly, the two buoys deployed in the Strait of Hormuz stopped transmitting within a few hours. All buoys on the southern side of the central Persian Gulf drifted in a southerly direction and either landed on shore or were heading that way before they terminated. In the northern part of the central Gulf almost no net drift was recorded over several weeks. Mean drift in this region ranged from 0.6 to 2.5 $\mathrm{cm\,s^{-1}}$.

The four ECOCAP buoys (3380, 5237–5239) followed a counter-clockwise circulation pattern and substantiated a counter-clockwise circulation theory. While it is generally accepted that the circulation in the northern Gulf follows a counter-clockwise circulation, some computer models have predicted a reverse direction. Spreading was exceptionally small: during the first 33 days of their deployment (after which buoy 5238 went off the air) the mean spread between the buoys was less than 4 km. Later the pattern broke apart: one buoy drifted onto the beach and the other two continued down the coast towards Qatar. We expect a similar behavior by an oil spill, and previous spills along the Iranian coast, especially the Nowruz spill and a spill at Kharg Island, did indeed drift westward to impact the Kuwait and Saudi Arabian coast.

A complex, double-gyre circulation pattern in the Gulf of Oman was indicated by buoys 9450, 9451, and 9460 (Fig. 26). Buoy 9450 was released on day 58, near the coast of Oman, and it followed a complex path. During the first weeks it wandered around the western Gulf of Oman, alternating between clockwise and counter-clockwise cycles. At one point it was swept into a large clockwise path that took it from Iran almost to Oman, and then out into the Arabian Sea. Buoy 9451, released on day 59, near the coast of Iran, was swept into a basin-scale counter-clockwise gyre before it, too, was carried out to sea. Buoy 9460, released in June on day 156, also moved in a clockwise direction along the coast of Oman and into the Strait of Hormuz. The large arrows in Fig. 26 show a proposed pattern for the two large counter-rotating, gyre-like features. The intersection of the two gyres occurred in a known region of coastal upwelling along the Iranian coast. The gyres pull cold coastal water offshore of Iran in a spout-like feature which is often seen along cuspate, coastal-upwelling coastlines. The cold-water spout in Fig. 26 is shown by the hatched area which was taken from an AVHRR, SST satellite image. Cold-water features such as these are regularly seen in AVHRR images of the Gulf of Oman.

Intercomparisons between the different buoys provided some confidence in the usability of the tracklines. We took the opportunity to compare the two oil-spill buoys with the Davis and the CMOD buoys (Fig. 27). The Davis buoy reflected the water motion at a depth of 0.5 m, while the CMOD buoy drag was centered at approximately 5 m. Nevertheless, the two buoys

tracked very well. The two oil spill buoys tracked almost identically, but went in a much different direction than the deeper-drogued pair, reflecting the much stronger wind component.

Six buoys, 9464–9469, were deployed in the north-central Inner gulf for the purpose of defining the overall circulation there, and with the additional goal of estimating the mean and turbulent mixing there. A surprise was the almost negligible drift and dispersion displayed by all six buoys. In spite of strong wind events and 20 km tidal excursions, these buoys remained tightly grouped for weeks after deployment. This apparent "low energy" area is described in a paper by Lehr et al. (1993). The situation is well represented in Table 4. With the exception of buoy 9466 which reported only four days, the buoys reported from 48–99 days and during that period, which included several extreme wind events, the mean, absolute speed was 18.9 ± 2 cm s^{-1} but the mean, vector-average speed was only 0.07 ± 0.02 cm s^{-1}. Thus, the net displacement was less than 0.5% of the total motion.

5 Conclusions

Measurements and models have the same general findings: (a) The inflow current along the Iranian coast is weakened by Shamal winds in the winter, but in the summer it strengthens and extends almost to the head of the Persian Gulf. (b) A cyclonic circulation gyre fills the southern Gulf and is driven by the inflowing surface water through the Strait of Hormuz. (c) Runoff from Shatt Al-Arab in the northwest Gulf maintains a cyclonic circulation there that would otherwise by anti-cyclonic. (d) A southward coastal jet exists between the head of the Gulf and Qatar, and extends east of Qatar, depending on the wind.

The mean wintertime surface current pattern in the southern Persian Gulf (Fig. 28) is the most widely known current pattern. The flow is predominantly density driven with surface flow inward from the Strait of Hormuz and adjacent to the Iranian coast. A southward coastal flow is present along the entire southern coast of the Persian Gulf. The flow stagnates east of Qatar, where high evaporation and sinking forms a dense, bottom flow to the northwest and out of the Strait of Hormuz.

The northern Gulf circulation is predominantly wind driven, with surface flow along both coasts in a southerly direction. Along Iran, the coastal flow is intensified by baroclinic forcing produced by low-density, river outflow. In the north-central Gulf a northerly return flow completes the wind-induced secondary circulation. The secondary circulation balances wind-drift in the surface water and creates a region of very low net drift. Circulation north and south of this low-energy region (marked by double arrows in Fig. 28) is variable and sensitive to winds. Flow at the north end can be easterly or westerly, clockwise or counterclockwise circulation, and to the south of the low-energy area will move northerly or southerly. The northern extent of the surface inflow marks a balance between the baroclinic forcing toward the north and the southward wind stress. Dashed lines in Fig. 28 mark the approximate limit of the inflow water. In the summer, the inflow is recognizable as far north as 28°N. Outflow from the Shatt Al-Arab is carried by the counter-clockwise circulation in a westerly direction and down the Kuwait and Saudi Arabian coast.

Circulation in the Gulf of Oman is dominated by a clockwise gyre in the west and a counter-clockwise gyre in the east. The interface between the two counter-rotating gyres is a region of upwelling along the Iranian coast. The circulation pattern seems to exist in winter and summer, but its strength and the upwelling depend on prevailing winds.

Recommendations: During the First Scientific Workshop on the results of the *Mt. Mitchell* Cruise, held in Kuwait from 24–28 January, 1993, oceanographers met to review the physical oceanographic findings of the cruise and to produce a prioritized set of research goals for the future. The recommendations of that meeting are given below.

1. Strait of Hormuz. The flow in and out of the Strait of Hormuz reflects the estuarine exchange of the Gulf with the world's oceans. Very little is known of the currents here. Models depend heavily on assumptions about this exchange, and until direct measurements in this region are available, models and flushing estimates will be inaccurate.

   The goal of direct measurements in the Strait of Hormuz is both terribly important and extremely difficult to accomplish. The high volume of ship traffic combined with extensive bottom-trawl fishing make this region very risky for moored instrumentation. Shipboard measurements or drifting buoys would be difficult to interpret. The strong tides mask the important yet weak residual currents, and the currents vary widely across the Strait.

2. Northern Persian Gulf. The circulation here must be defined for different winds and seasons. The variability of the Iranian coastal flow must be better understood. This task requires more moored, current-meter studies over all the seasons of a year. Wind measurements are a necessary part of such a study.

3. Wind stress and energy fluxes. We need over-the-water, scientific-quality meteorological measurements at several locations in the RSA. Accurate evaporation estimates are required to compute flushing and residence times. Wind stress drives oil-spill dispersion and the very important secondary flow in the north. Over-the-water records of a year or longer can be correlated with coastal stations so accurate transfer functions can be derived.

   Of all the tasks listed here, quality, over-the-water, meteorological measurements are the easiest to achieve. Instrumentation is available, excellent platforms are available, and satellite measurements are seldom troubled by clouds. Immediate steps should be taken towards this goal. A numerical model should be developed in parallel to the measurement study. In this way the model would be tuned by the measurements so that it will be able to make good quality estimates of wind fields in the absence of measurements.

4. Central Gulf. A better understanding of the circulations in the Gulf of Oman, their seasonal and spatial variations, and the exchange of water with the Strait of Hormuz and the Arabian Sea is needed. A combination of current-meter moorings and wind stations is required in a multi-year study.

ACKNOWLEDGEMENTS

The NOAA expedition of the *Mt. Mitchell* was co-sponsored by the International Oceanographic Commission (IOC), the United Nations Environmental Programme (UNEP), and the Regional Organization for the Protection of the Marine Environment (ROPME), all of whom provided assistance in planning and financing the expedition. Special thanks are also extended to the Marine Spill Response Corporation (MSRC) for considerable financial and scientific contribution.

The engineers and workers at the NOAA Atlantic Marine Center deserve special thanks for their relentless efforts to outfit and prepare the *Mt. Mitchell* for this voyage. Dennis Shields and Robert Perry deserve a vote of thanks for installing the SCS system on the ship in such a short time. All systems worked well and the quality of data obtained from the ship was excellent. Captain Permenter and his crew are thanked for their efforts to complete the entire suite of stations in spite of adverse weather conditions that prevented us from using the RHIBs. Paul Moen, the Field Operations Officer, worked long hours, often sacrificing sleep to see that all work was completed properly. Dr. Robert C. Clark, the expedition leader, maintained a persistently unflappable and calm approach to difficult situations and thus made many potential problems disappear. His tenacity in mooring recovery attempts (M6 and M5) was exceptional.

Several key persons in NOAA management contributed enormously, both towards the cruise itself and towards data analysis afterwards. A special acknowledgement goes to Dr. John Knauss, who was NOAA Administrator during this period, for having the vision to recognize the importance of this research and the tenacity to put forward the ship and personnel, in times of restricted budgets, to make it a success. John Robinson, Director of the Gulf Program Office, worked diligently to accommodate the scientific needs and attend to endless logistical issues. Ms. Lisa Symmons provided thorough logistical support for the crew and scientists. Funding for research leading to this paper was provided by a grant from NOAA and with services support from Brookhaven National Laboratory.

6 References

Ackleson, Steven G., David E. Pitts, Kathryn D. Sullivan, and R. Michael Reynolds. (1992). Astronaut Observations of the Persian (Arabian) Gulf During STS-45. *Geocarto International* 7 (4): 59–68.

Argos, Service. (1988). *Users Manual*. Service Argos, Inc., Landover MD 20785, 56 pp.

Brewer, Peter G. and D. Dyrssen. (1985). Chemical Oceanography of the Persian Gulf. *Prog. Oceanography* 14: 41–55.

Congressional Research Service. (1992). *The Environmental Aftermath of the Gulf War*. U.S. Government Printing Office. ISBN 0-16-037720-X, Washington D.C., Prepared for the Committee on Environment and Public Works Gulf Pollution Task Force. Report S.Prt. 102-84. 74 pp.

Chao, Shenn-Yu, Timothy W. Kao, and Khalid R. Al-Hajri. (1992). A Numerical Investigation of Circulation in the Arabian Gulf. *Jour. Geophys. Res.* 97 (C7): 11219–11236.

Davis, Russ E. (1985a). Drifter Observations of Coastal Surface Currents During CODE: The Method and Descriptive View. *Journal of Geophysical Research* 90 (3): 4741–4755.

Davis, Russ E. (1985b). Drifter Observations of Coastal Surface Currents During CODE: The Statistical and Dynamical Views. *Journal of Geophysical Research* 90 (3): 4756–4772.

Emery, K.O. (1956). Sediments and water of Persian Gulf. *Bull. Amer. Ass. Petrol. Geol.* 40 (10): 2354-2383.

Flagg, C.N., John A. Vermersch, and Robert C. Beardsley. (1976). *1974 M.I.T. New England Shelf Dynamics Experiment (March, 1974) Data Report. Part II: The Moored Array*. Woods Hole Institution of Oceanography, Woods Hole MA., 76-1. 110 pp.

Galt, J.A. (1983). Trajectory analysis and simulation of Oil Spill Movement. In: El-Sabh, Mohammed I. (ed). *Oceanographic Modeling of the Kuwait Action Plan (KAP) Region*. UNESCO reports in Marine Science, 28. Paris. 46–54.

Galt, J.A., D.L. Payton, G.M. Torgrimson, and G. Watabayashi. (1983). Applications of Trajectory Analysis for the Nowruz Oil Spill. In: El-Sabh, Mohammed I. (ed). *Oceanographic Modeling of the Kuwait Action Plan (KAP) Region*. Unesco reports in Marine Science, 28. Paris. 55–66.

Galt, J.A. (1992). *Report of Activities – Leg III of the* Mt. Mitchell *Expedition*. National Oceanic and Atmospheric Administration, HMRAD, HMRAD 92-9, Seattle WA USA. 50 pp.

Hajri, Khalid Al-. (1990). *The Circulation of the Arabian (Persian) Gulf: A Model Study of its Dynamics*. The Catholic University of America, Washington D.C., Ph.D. Dissertation (also available through UMI Dissertation Information Service, Order Number 9106378). 218 pp.

Horton, C., M. Clifford, D. Cole, J. Schmitz, and L. Kantha. (1992). Operational modeling semienclosed basin modeling at the Naval Oceanographic Office. *Oceanography* 5 (1): 69–72.

Hughes, P. and J.R. Hunter. (1979). *A Proposal for a Physical Oceanography Program and Numerical Modeling of the KAP Region*. UNESCO, Div. Mar. Sci., Paris, MARINF/27, 16 Oct. 1979. 102 pp.

Hunter, J.R. (1983). A Review of the Residual Circulation and Mixing Processes in the KAP Region, with Reference to Applicable Modeling Techniques. In: El-Sabh, Mohammed I. (ed). *Oceanographic Modeling of the Kuwait Action Plan (KAP) Region*. UNESCO reports in Marine Science, 28. Paris. 37–45.

Hunter, J.R. (1983). Aspects of the Dynamics of the Residual Circulation of the Arabian Gulf. In: Gade, H.G., A. Edwards, and H. Svendsen (ed). *Coastal Oceanography*. Plenum Press. New York/London. 31–42.

Lardner, R.W., M.S. Belen, and H.M. Cekirge. (1982). Finite difference model for tidal flows in the Arabian Gulf. *Comp. & Maths. with Appls.* 8(6): 425–444.

Lardner, R.W., W.J. Lehr, R.J. Fraga, and M.A. Sarhan. (1987). Residual Circulation in the Arabian Gulf. I: Density-driven flow. *The Arabian Journal for Science and Engineering* 12 (3): 341–354.

Lardner, R.W., W.J. Lehr, R.J. Fraga, and M.A. Sarhan. (1988a). A model of residual currents and pollutant transport in the Arabian Gulf. *Appl. Math. Modelling* 12: 379–390.

Lardner, R.W., R.J. Fraga, W.J. Lehr, and M.A. Sarhan. (1988b). Residual Circulation in the Arabian Gulf. II: Wind-driven flow. *The Arabian Journal for Science and Engineering* 13 (3): 411–423.

Lardner, R.W. and S.K. Das. (1991). On the computation of flows driven by density gradient: Residual currents in the Arabian Gulf. *App. Math. Modelling* 15: 282–294.

Lardner, R.W., A.H. Al-Rabeh, N. Gunay, M. Hossain, R.M. Reynolds, and W.J. Lehr. (1993). Computation of the Residual Flow in the Arabian Gulf Using the Mt Mitchell Data and the KFUPM/RI Hydrodynamical Models. *Proceedings of the Scientific Workshop on Results of the* Mt. Mitchell *Cruise*, Regional Organization for the Protection of the Marine Environment, Kuwait, pp in preparation.

Lehr, W.J. (1984). A brief survey of oceanographic modelling and oil spill studies in the KAP region. In: El-Sabh, Mohammed I. (ed). *Oceanographic Modeling of the Kuwait Action Plan (KAP) Region*. UNESCO reports in Marine Science, 28. Paris. 4–11.

Lehr, W.J., R. Overstreet, and Debra Simecek-Beatty. (1993). Analysis of the drifters released during the Mt. Mitchell cruise for the purpose of calculating differential kinetic properties of the ROPME Sea Area. *Proceedings of the Scientific Workshop on Results of the* Mt. Mitchell *Cruise*, Regional Organization for the Protection of the Marine Environment, Kuwait, pp submitted.

Le-Provost, C. (1984). Models for Tides in the KAP region. In: El-Sabh, Mohammed I. (ed). *Oceanographic Modeling of the Kuwait Action Plan (KAP) Region*. UNESCO reports in Marine Science, 28. Paris. 37–45.

Meshal, A.H. and H.M. Hassan. (1986). Evaporation from the Coastal Waters of the Central Part of the Gulf. *Arab Journal of Sci. Res.* 4 (2): 649-655.

National Oceanic and Atmospheric Administration. (1993). *Expedition Report:* Mt. Mitchell *Expedition to the ROPME Sea Area February- June, 1992*. Intergovernmental Oceanographic Commission of the United Nations Educational, Scientific and Cultural Organization, Paris, . 58 pp.

Perrone, T.J. (1981). *Winter Shamal in the Persian Gulf*. Naval Environmental Prediction Research Facility, Monterey CA, I.R.-79-06. approx 23 pp.

Privett, D.W. (1959). Monthly charts of evaporation from the North Indian Ocean, including the Red Sea and the Persian Gulf. *Q.J. Roy. Meteor. Soc.* 85: 424–428.

Reynolds, R. Michael. (1992a). *Report of Activities – Leg I of the* Mt. Mitchell *Expedition*. National Oceanic and Atmospheric Administration, HMRAD, HMRAD 92-9, Seattle WA USA. 110 pp.

Reynolds, R. Michael. (1992b). *Report of Activities – Leg VI, A/B of the* Mt. Mitchell *Expedition*. National Oceanic and Atmospheric Administration, HMRAD, HMRAD 92-10, Seattle WA USA. 110 pp.

Tawflg, I. Nizar. (1987). Satellite-Tracked Buoy Activities in Saudi Arabia. *Coastal Zone '87 Proceedings*, Presented at Coastal Zone '87 Conference, , pp 441–452.

Williams, R.O. (1991) *Massive Oil Spill in the Persian Gulf.* Informal report, Saud Arabian Oil Company, Dhahran, Saudi Arabia, 8 pp.

Table 1: The 'at sea' times for the various legs of the *Mt. Mitchell* cruise. The times specify when the ship was away from the dock according to the ship log. Times in universal coordinated time (UTC).

LEG	START	STOP	PRIMARY ACTIVITIES
1	57 0700	71 1800	Muscat–Jubail: CTD, drifter survey, moorings, sediments
2	77 0900 92 1200	91 1000 97 0800	Jubail–Jubail: Oil impact at Abu Ali Jubail–Manamma
3	105 1300	111 0800	Manamma–Kuwait: Intense CTD arrays on Iran coast
4	115 1400 116 1500	116 1300 124 0700	Kuwait–Kuwait: Fisheries Kuwait–Doha
5	128 1300	137 0600	Doha–Kuwait: Reef ecology, benthic biology
6a	141 0900	151 0600	Kuwait–Abu Dhabi: Repeat Leg I CTD survey, sediments, microfauna
6b	154 0600	158 0600	Abu Dhabi–Muscat: Complete Leg VI survey
7	160 0600	164 1300	Muscat–Salallah: Hydrographic and biological study of the Oman eastern seaboard.

Table 2: Physical Oceanography measurements taken during the *Mt. Mitchell* cruise.

MEASUREMENT	NUMBER	DESCRIPTON
CTD – basin wide	≈ 300	Large scale temperature, salinity and density fields in winter (Feb–Mar) and early summer (May–June).
CTD – Iran coast	≈ 225	Intensive survey of three Iranian coastal regimes where river outflow creates a unique coastal circulation.
Moored current meters	11	Seven moorings with 17 meters deployed and five moorings with 11 records recovered. Study focussed on estuarine surface inflow-along the Iranian Coast.
drifting buoys	32	Argos-tracked buoys to sample circulation patterns and investigate mixing processes.
satellite AVHRR	≈ 120	AVHRR images (4 bands) for the year days 57–165 provide qualitative picture of circulation and mixing proceses.
shuttle photography	≈ 120	Film and electronic still camera images taken during shuttle flight STS-45 provide visible, high-resolution pictures of coastal features.
ship computer system (SCS)	90 days	Continuous digitized time series of weather, navigation, and oceanographic measurements.

Table 3: Current meter time series.

METER SN	DEPTH (m)	START DAY (ddd hhmm)	END DAY (ddd hhmm)
Mooring M2: 26 22.44N, 55 45.66E, depth=94.4 m			
2265	10	61 2228	150 0908
7251†	30	62 2216	150 0916
2171	84	61 2207	150 0927
Mooring M3: 27 03.79N, 52 22.75E, depth=81 m			
5988	10	65 0733	148 1233
5431	24	65 0732	148 1251
6674†	40	65 0727	148 1247
3214	71	65 0731	148 1251
Mooring M4: 26 50.40N, 51 58.57E, depth=69 m			
3176	15	64 2247	148 0927
2512	59	64 2229	148 0909
Mooring M5: 25 59.67N, 52 00.13E, depth=33 m			
6670†	21	64 1026	149 1506
Mooring M7: 27 11.09N, 51 19.46E, depth=76 m			
7027†	56	65 1645	148 0425

† Qatar meters

Table 4: Stastistics of the drifter program. The drogue depths for Davis, CMOD, and ECOCAP are 0.5, 5, and 3 m respectively. The LCD and SSD are oil spill drifters and are designed to move as a surface slick.

ID	TYPE	DDHH	LAT	LONG	T	ΔL	$\int \mathrm{d}L$	$\overline{V}$	$\overline{S}$	$(\overline{V}/\overline{S})$
9450	Davis	5821	24 45.5	57 07.3	1950	1479	278	3.96	21.07	0.19
9451	Davis	5903	25 23.8	57 56.5	453	495	188	11.56	30.37	0.38
9452	Davis	6009	26 41.8	56 12.5	42	13	4.4	2.89	8.59	0.34
9453	Davis	6009	26 23.8	56 11.4	15	9	8	14.93	17.51	0.85
9454	Davis	6012	26 29.4	54 56.0	33	8	3	2.64	7.12	0.37
9455	Davis	6015	25 57.1	55 08.0	729	542	15	0.56	20.65	0.03
9456	Davis	6018	25 39.4	55 17.9	6	45	45	208	208	1.0
9457	Davis	6500	26 16.7	52 47.4	552	367	118	5.93	18.45	0.32
9458	Davis	6500	26 40.9	52 09.0	144	73	13	2.52	14.05	0.18
9459	Davis	6500	27 07.3	52 33.9	456	237	20	1.22	14.43	0.08
9460	Davis	15612	24 57.2	56 49.8	444	350	129	8.05	21.89	0.37
9461	Davis	7000	27 38.3	50 36.6	1203	784	144	3.32	18.09	0.18
9462	Davis	7012	27 53.2	40 59.2	273	195	21	2.10	19.83	0.11
9463	Davis									
9464	Davis	6621	28 48.8	49 25.2	2379	1529	194	2.26	17.85	0.13
9465	Davis	6621	28 48.8	49 25.2	1155	858	13	0.32	20.63	0.02
9466	Davis	6621	28 48.8	49 25.2	99	57	9	2.53	16.12	0.16
9467	Davis	6621	28 48.8	49 25.2	1347	965	16	0.33	19.89	0.02
9468	Davis	6621	28 48.8	49 25.2	1227	870	7	0.17	19.69	0.01
9469	Davis	6621	28 48.8	49 25.2	1755	1193	56	.88	18.89	0.05
1723	CMOD	6212	24 57.9	53 44.9	270					
1725	CMOD	6203	25 39.2	55 50.1	240	184	26	3.04	21.25	0.14
1726	CMOD									
1727	CMOD	15800	24 57.2	53 47.3	405	334	145	9.97	22.93	0.43
2048	CMOD	7200	27 38.3	56 49.8	1155	559	168	4.05	13.43	0.30
2049	CMOD	6921	27 53.2	50 36.6	435	315	125	8.01	20.10	0.40
3380	ECOCAP	10921	29 35.0	40 59.2	1134	877	156	3.82	21.49	0.18
5237	ECOCAP	10921	29 35.0	40 59.2	1494	1174	242	4.50	21.83	0.21
5238	ECOCAP	10921	29 35.0	40 59.2	747	546	58	2.15	20.30	0.11
5239	ECOCAP	10921	29 35.0	40 59.2	1494	1183	222	4.12	22.00	0.19
9825	LCD	15621	24 57.2	56 49.8	123	99	58	13.12	22.39	0.59
14684	SSD	15621	24 57.2	56 49.8	123	105	58	12.99	23.82	0.55

ID = buoy identification number.
TYPE = design name.
DDHH = year day and hour of the first 'hit'.
LAT = deployment latitude (dd mm.m N).
LONG = deployment longitude (dd mm.m E).
T = total operation time (hrs).
ΔL = net displacement (km).
$\int \mathrm{d}L$ = integrated path length (km).
$\overline{V}$ = vector average velocity ($\mathrm{cm\,s^{-1}}$).
$\overline{S}$ = mean scalar speed ($\mathrm{cm\,s^{-1}}$).
$(\overline{V}/\overline{S})$ = ratio of speeds.

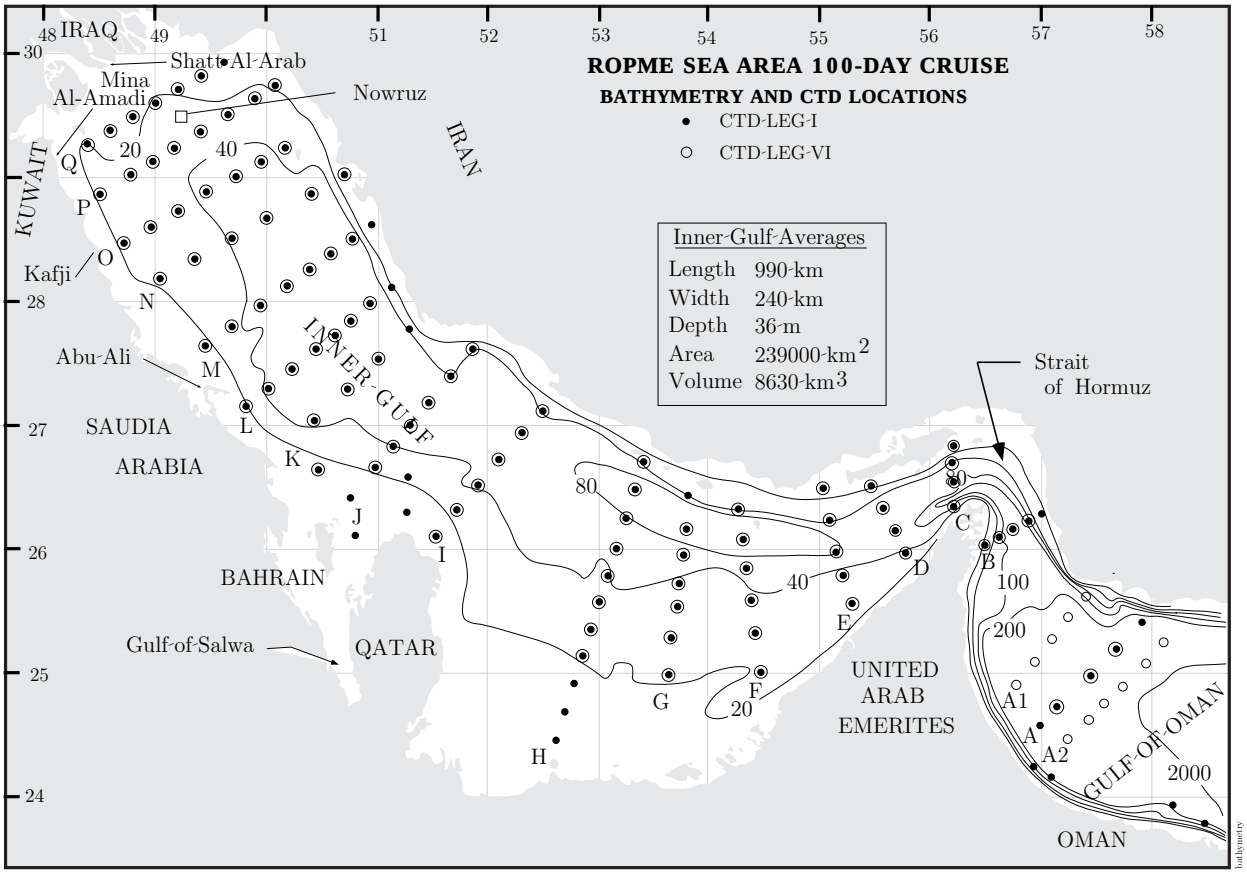

Figure 1: Bathymetric map of the ROPME Sea Area (RSA). The main bodies of water are the Persian Gulf, Strait of Hormuz, and the Gulf of Oman. CTD stations are shown: solid circles designate stations occupied on Leg I and open circles are stations occupied on Leg VI.

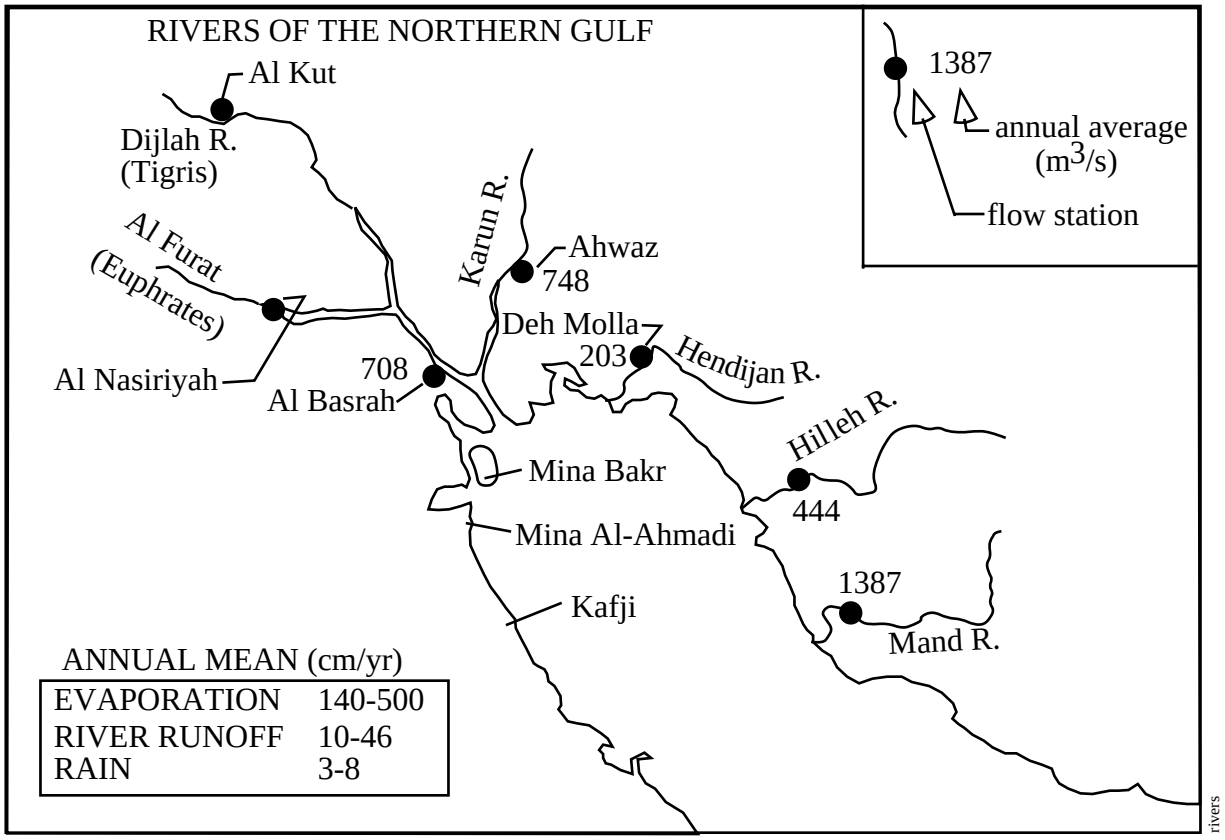

Figure 2: Map showing the major rivers into the northern RSA. Solid circles mark the locations of river flow stations. The annual-mean flow rates for each river are shown. Note, in the left inset, the evaporation exceeds runoff approximately by a factor of ten. Note also the considerable uncertainty in these estimates.

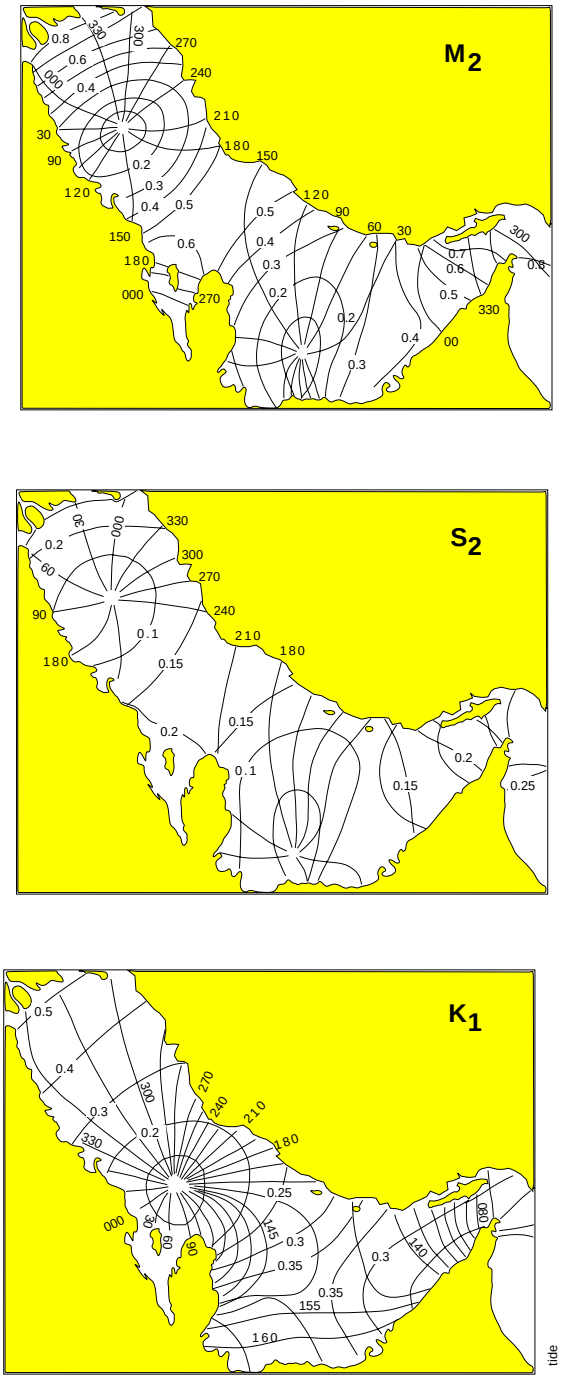

Figure 3: The M_2, S_2, and K_1 tidal constituents in the Persian Gulf (Lardner et al., 1982). Tide heights are shown in meters.

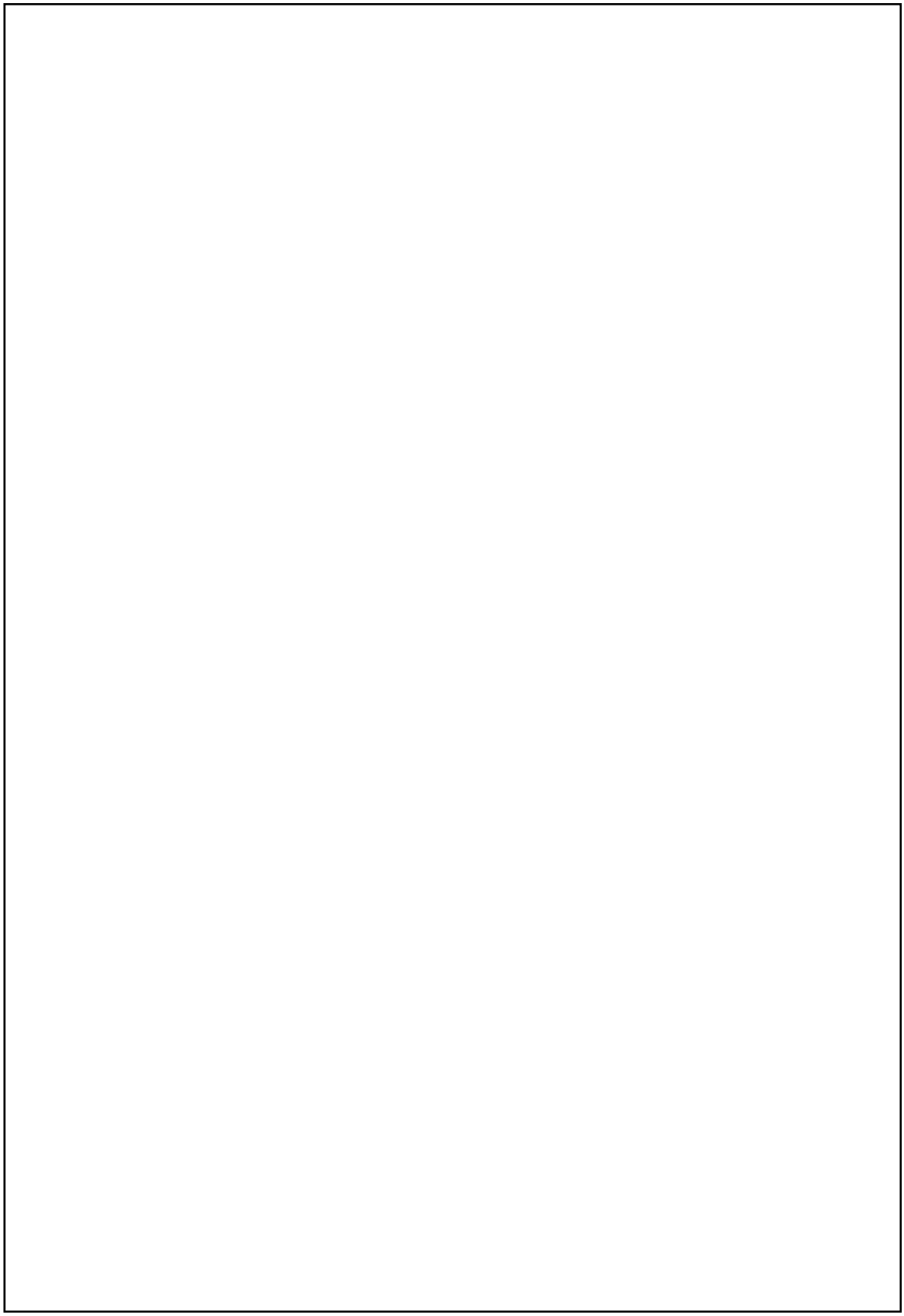

Figure 4: Color enhanced of AVHRR images for winter and summer conditions.

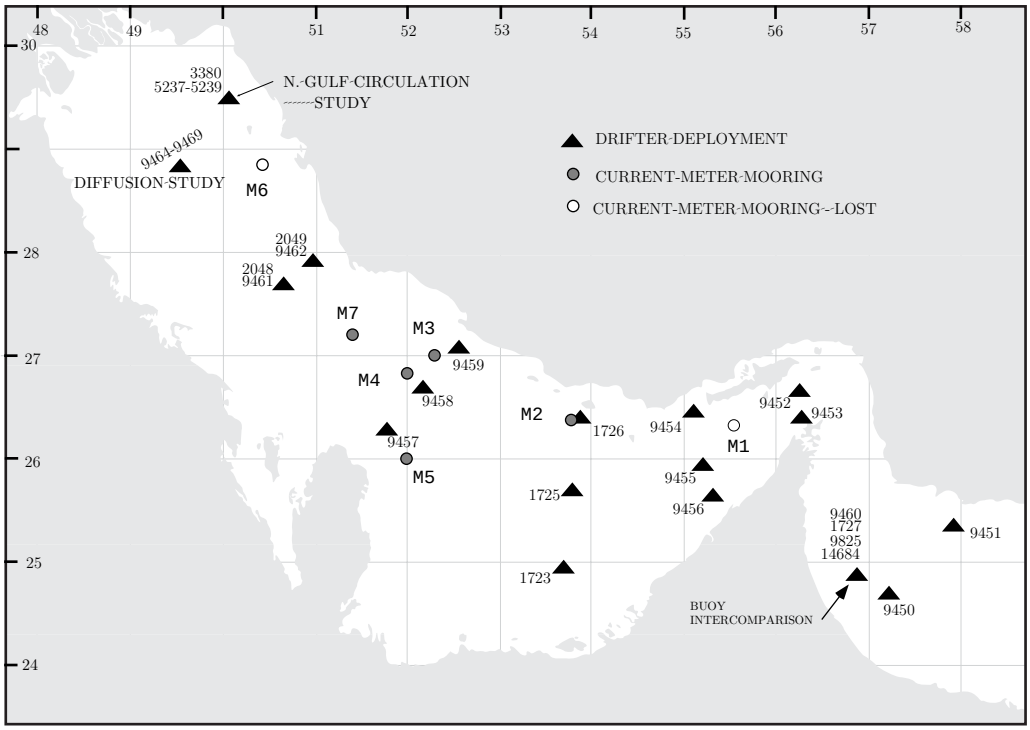

Figure 5: Map of physical oceanographic stations. Map of the RSA showing locations of the drifting buoy deployments and anchored mooring sites. Open circles mark moorings that were not recovered (M1 and M6) and filled circles mark recovered moorings. Solid triangles mark deployment sites for Argos drifters.

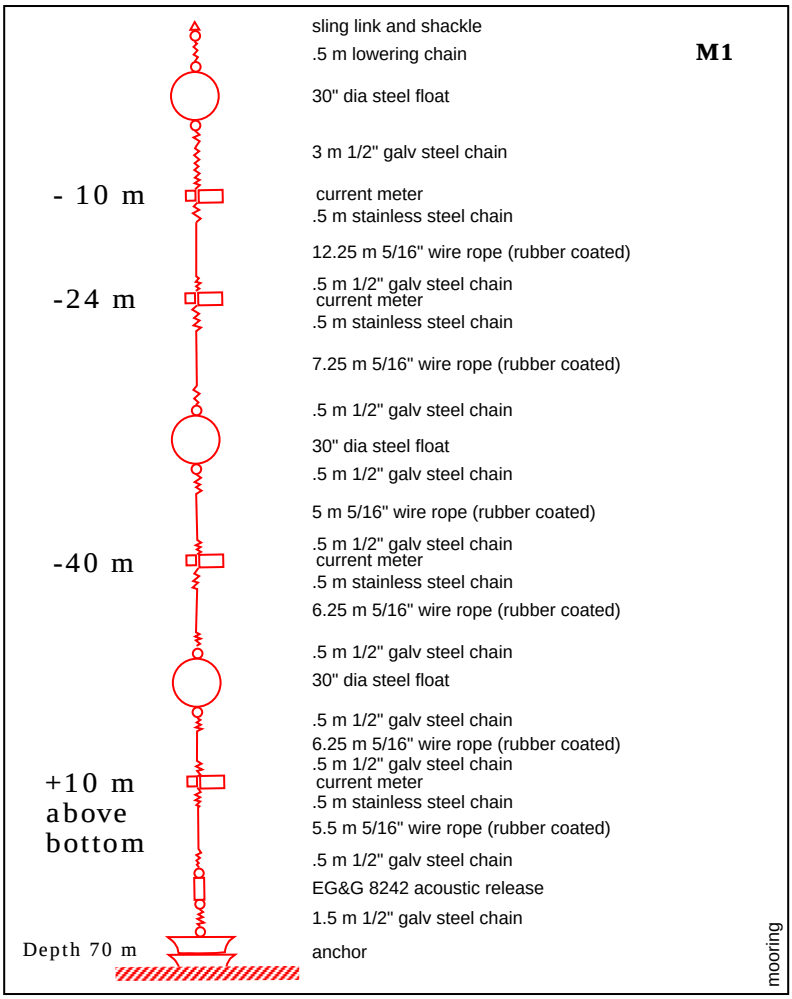

Figure 6: Typical current meter mooring. The mooring was specially designed for high ship traffic areas with a backup recovery system comprised of the acoustic release and several sub-surface floats distributed along the line. If the upper float is flooded, enough additional buoyancy is available from the other floats to bring the entire mooring to the surface.

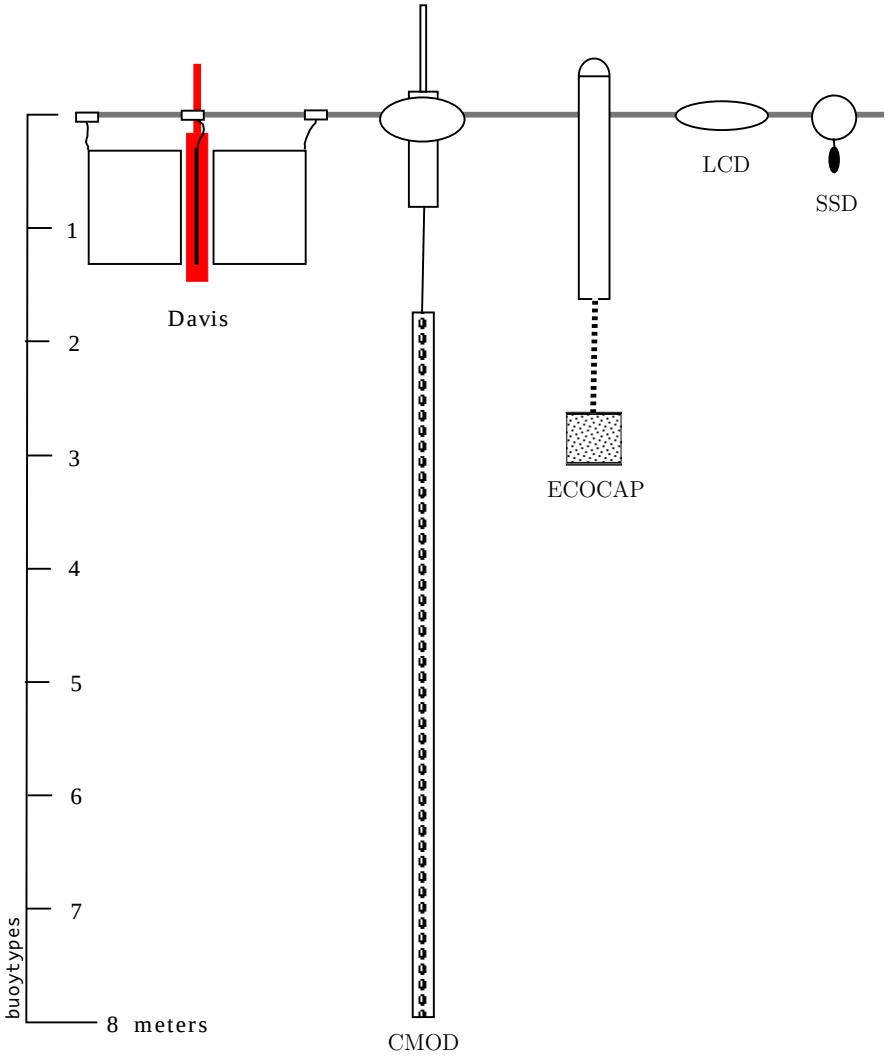

Figure 7: Five different types of drifter buoys used in the study.

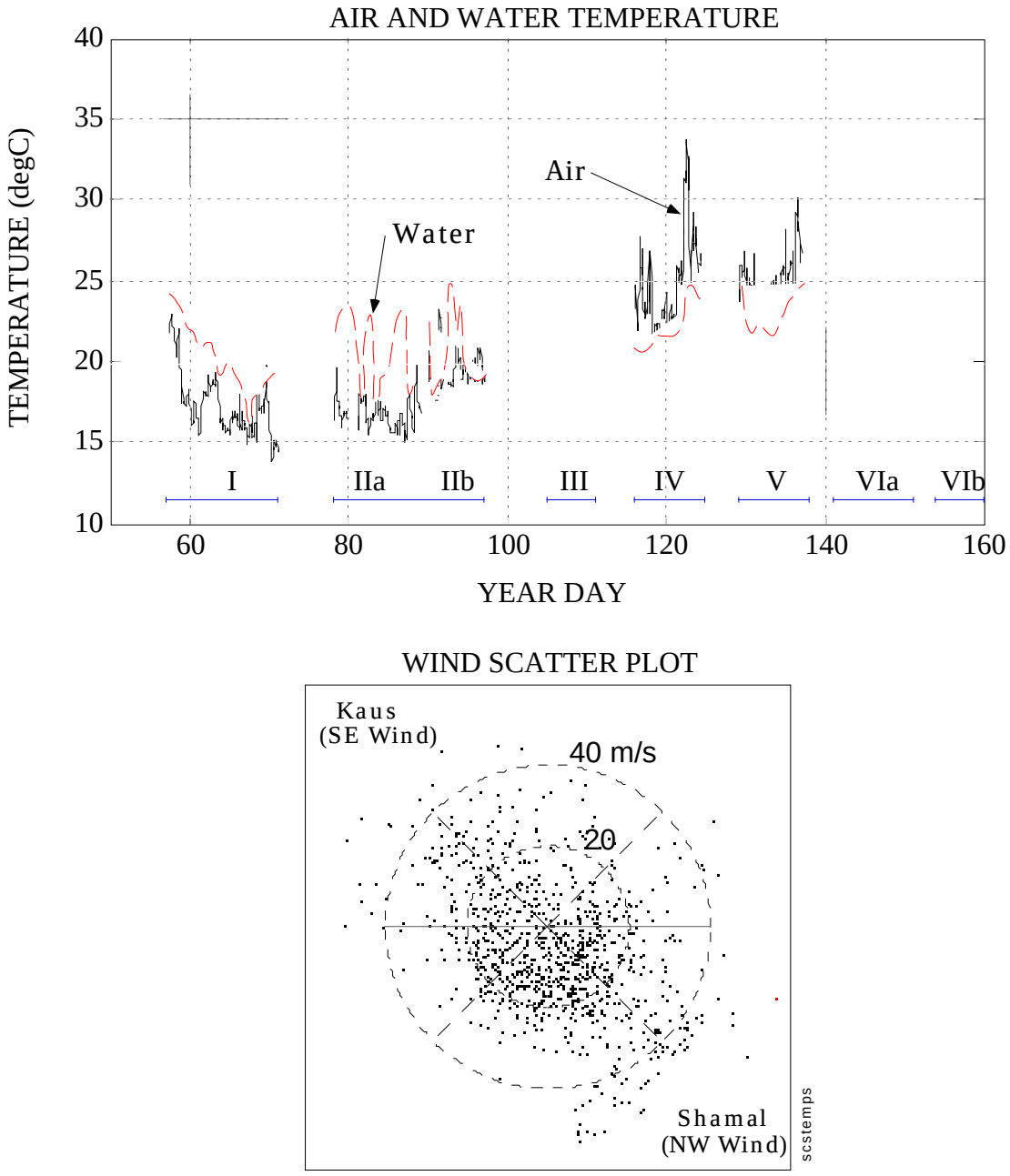

Figure 8: (upper) Comparison of air and water temperature measured on the *Mt. Mitchell*. Only data taken while the ship was at sea are shown. During Leg I and Leg II, water temperature was greater than air temperature which creates an unstable surface layer. During Leg IV and Leg V the air was warmer than the water implying a stable surface layer. (lower) A scatter plot of hour-average, wind vectors (in the direction of the wind flow) shows a preferred NW and SE direction, and occasional Shamal occurences of winds greater than 40 $\mathrm{m\,s^{-1}}$.

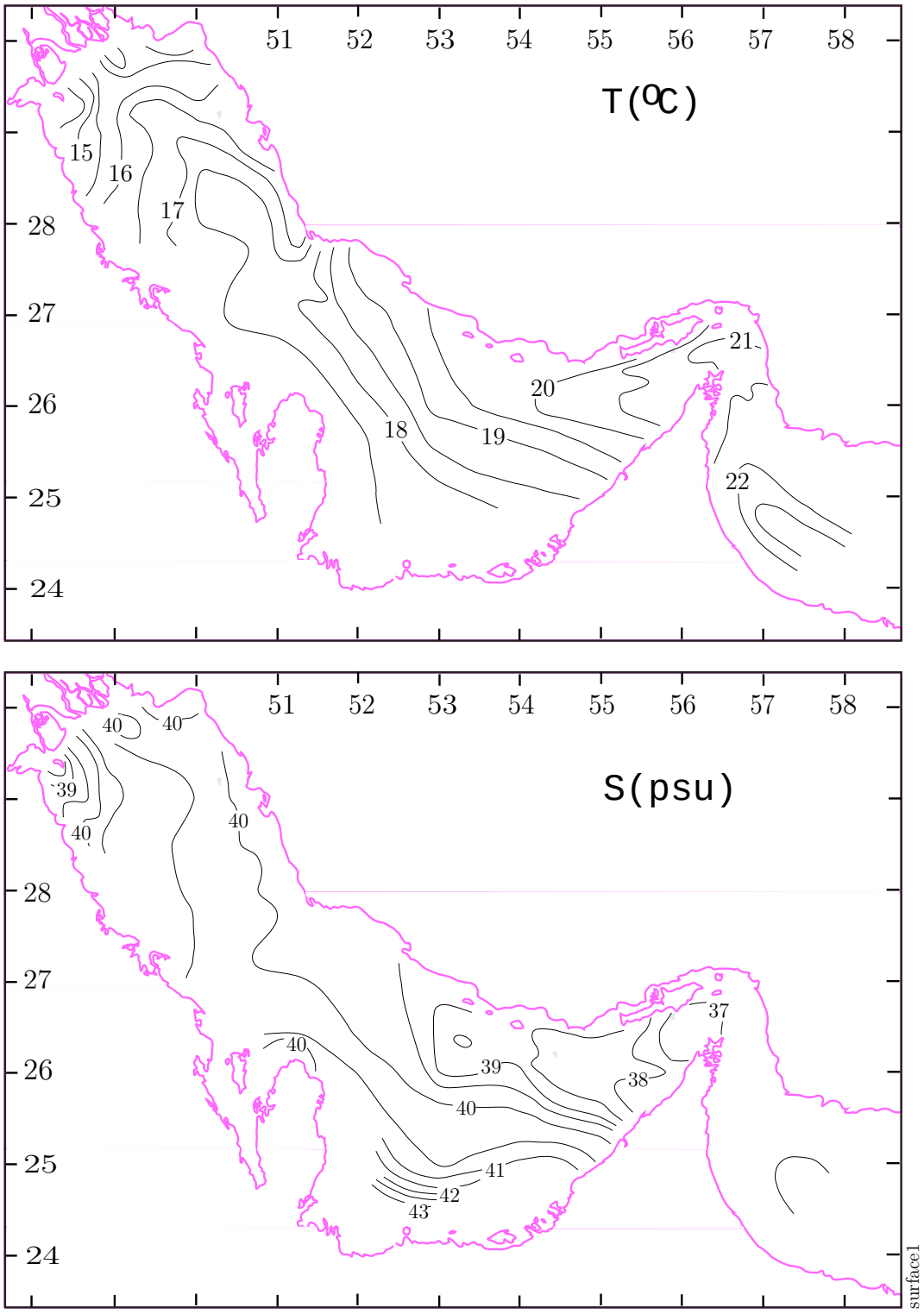

Figure 9: Maps of surface temperature and salinity for winter, Leg I.

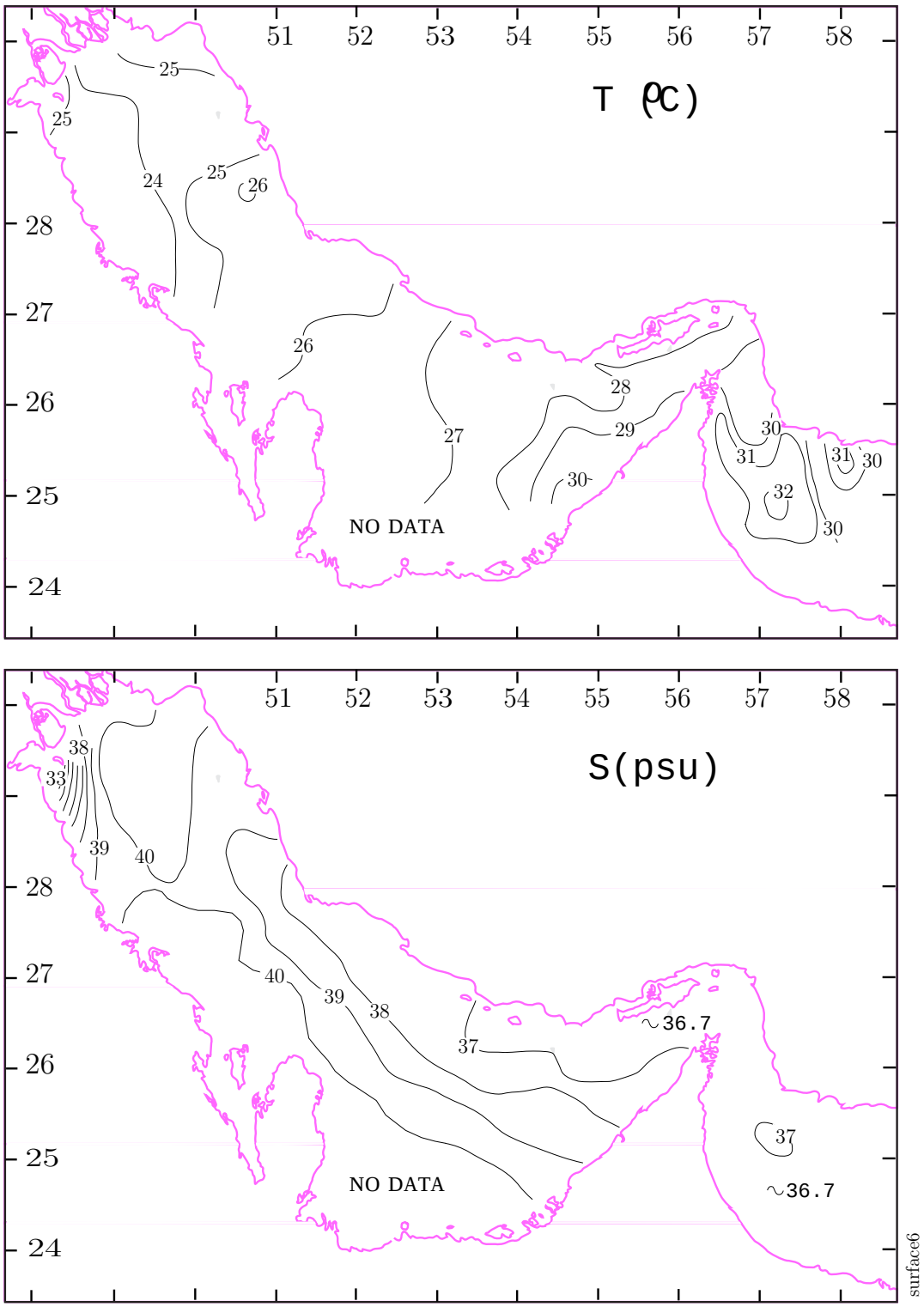

Figure 10: Maps of surface temperature and salinity for early summer, Leg VI.

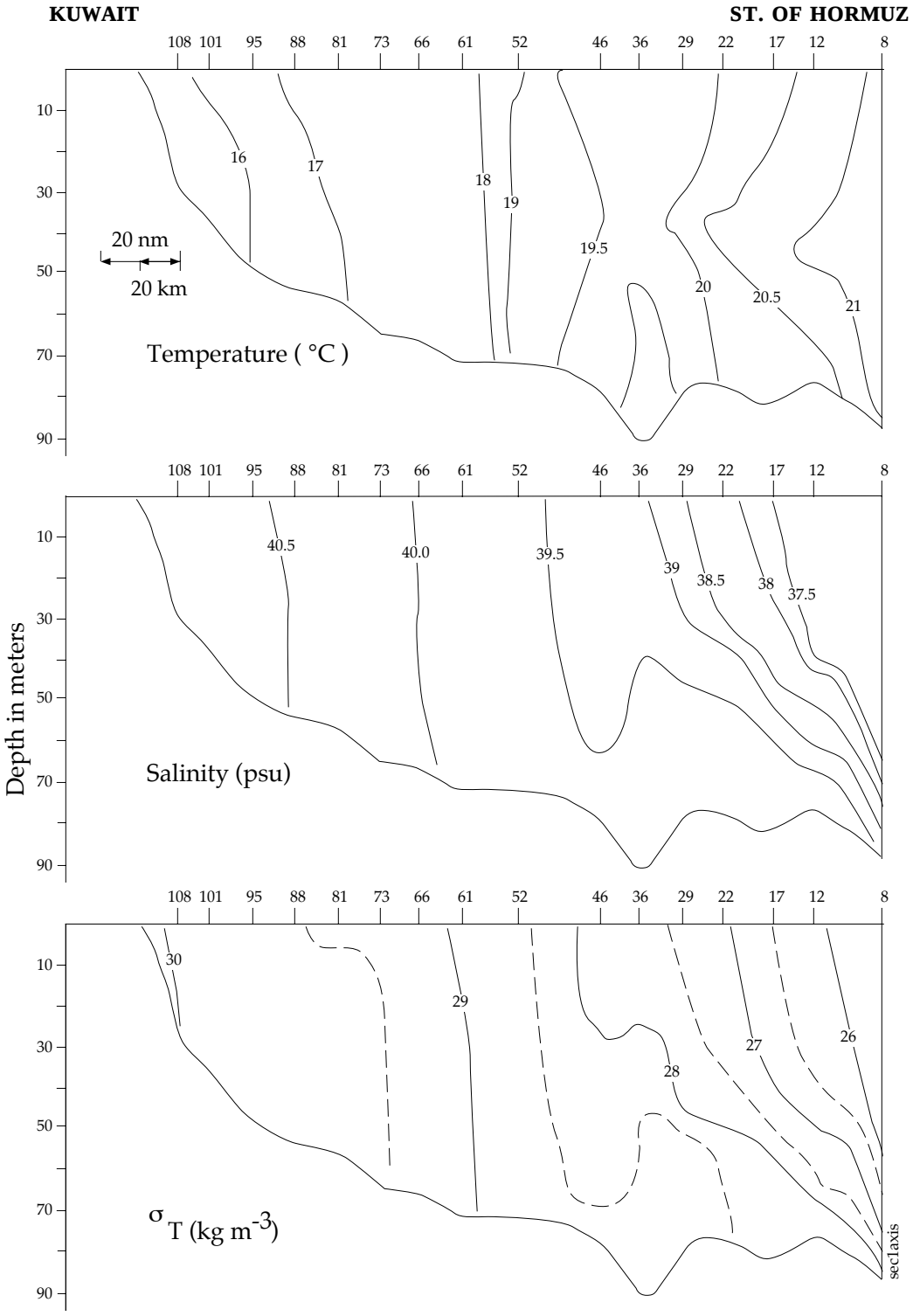

Figure 11: CTD cross section along the axis of the Persian Gulf from Leg I (winter) survey.

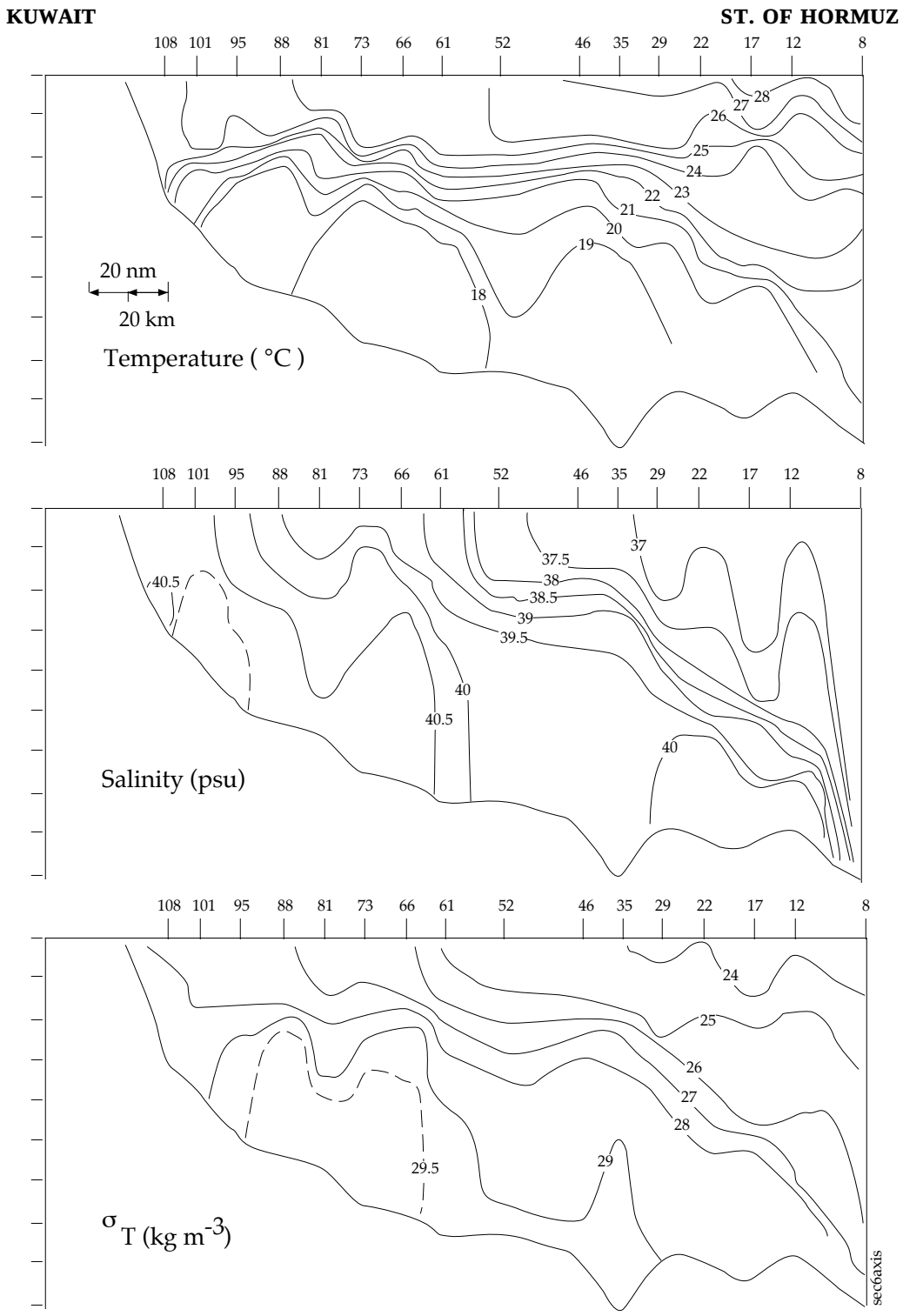

Figure 12: CTD cross section along the axis of the Persian Gulf from Leg VI (summer) survey.

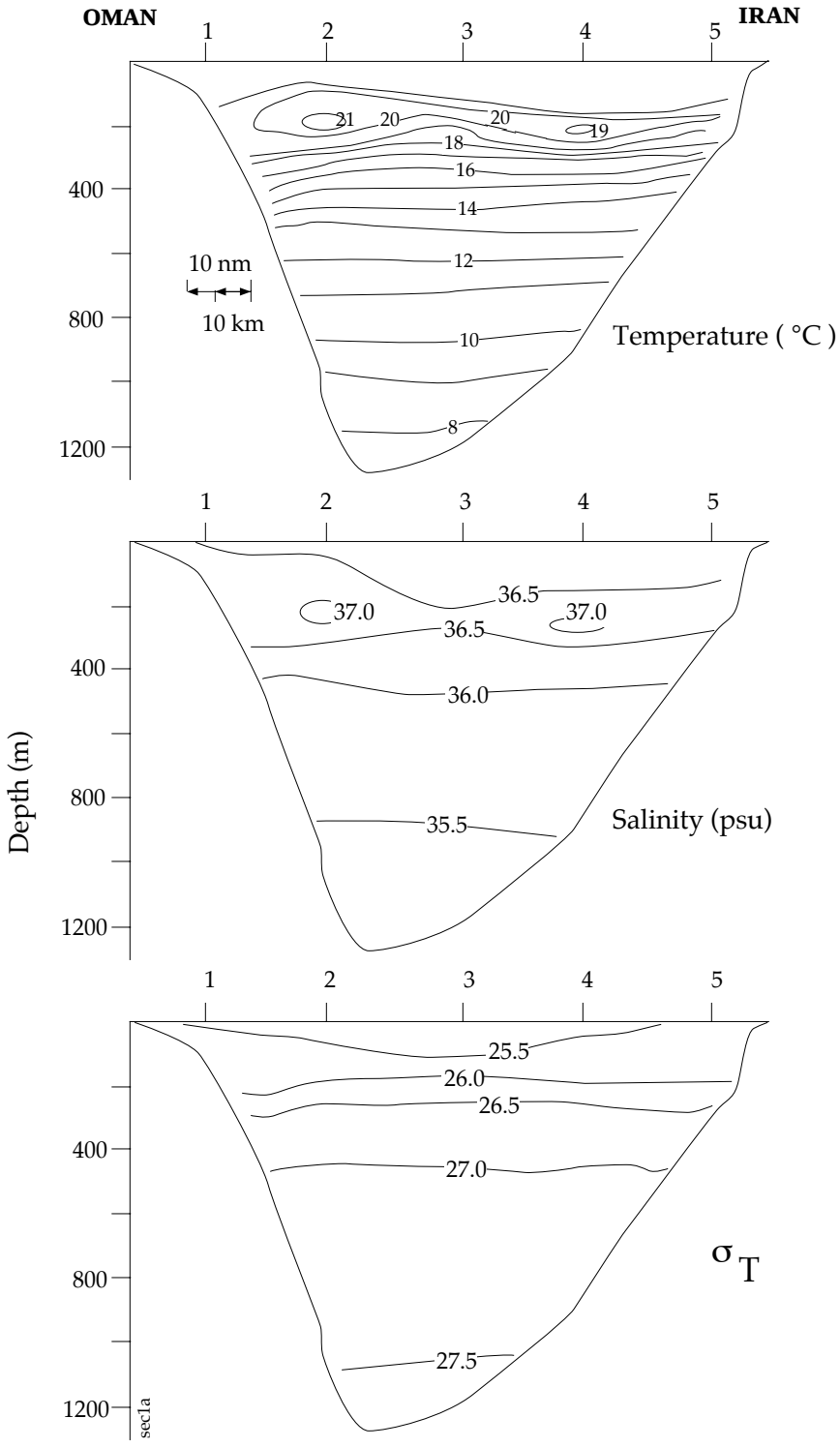

Figure 13: CTD cross section along line A in the Gulf of Oman during Leg I (winter).

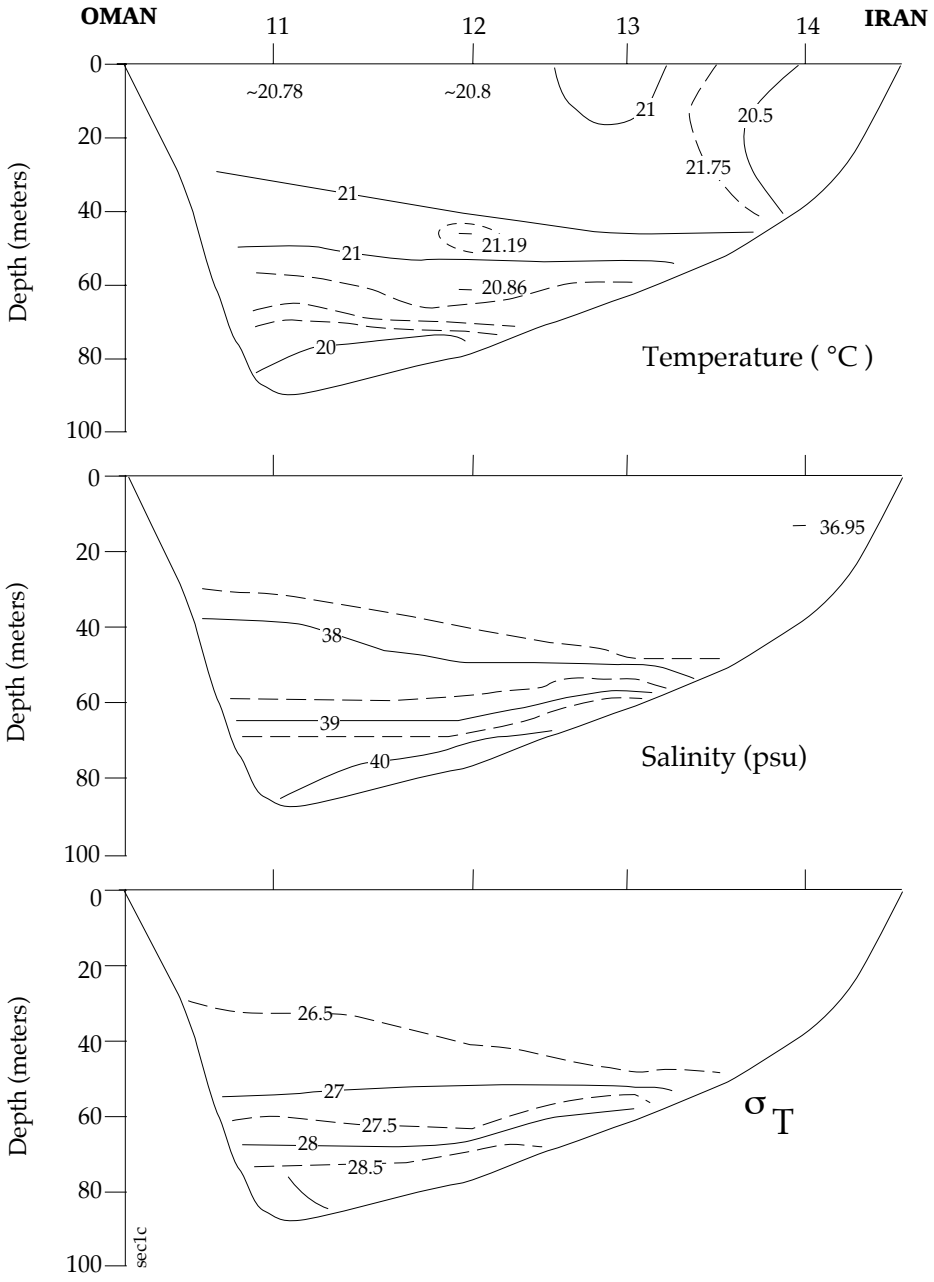

Figure 14: CTD cross section across the Strait of Hormuz, along line C, during Leg I (winter)

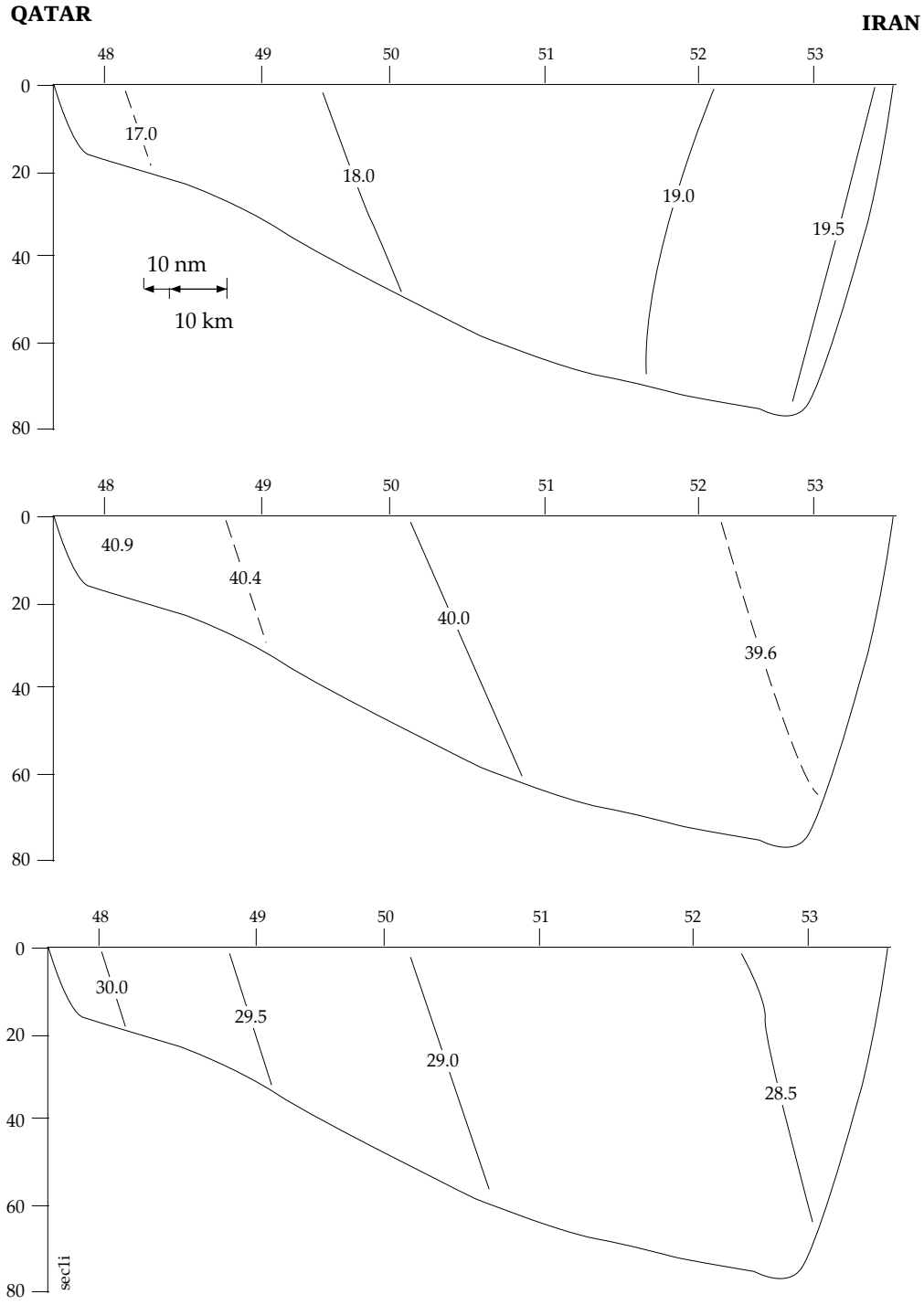

Figure 15: CTD cross section across the southern Persian Gulf along line I during Leg I (winter)

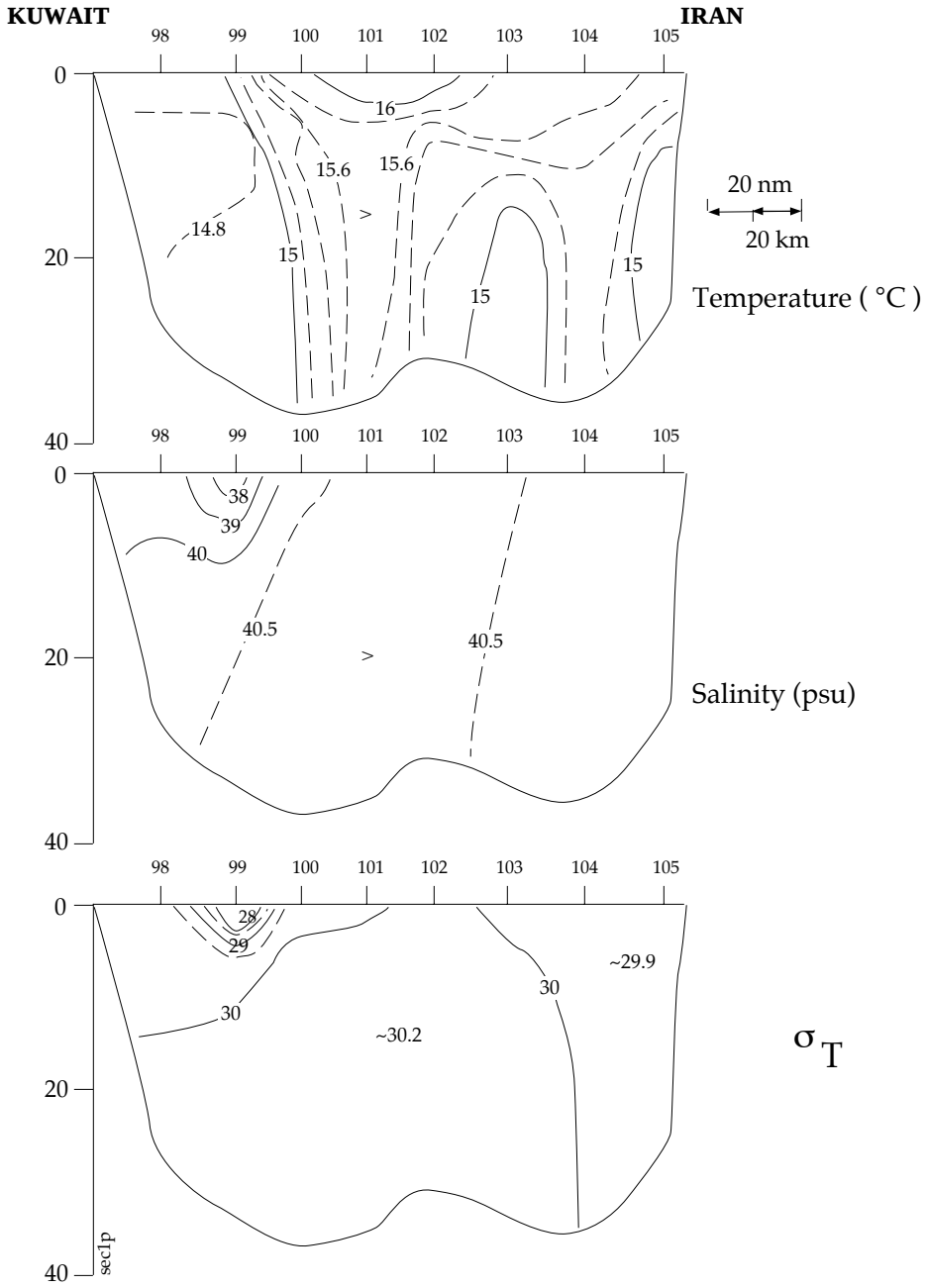

Figure 16: CTD cross section across the north-central Persian Gulf, along line P, during Leg I (winter)

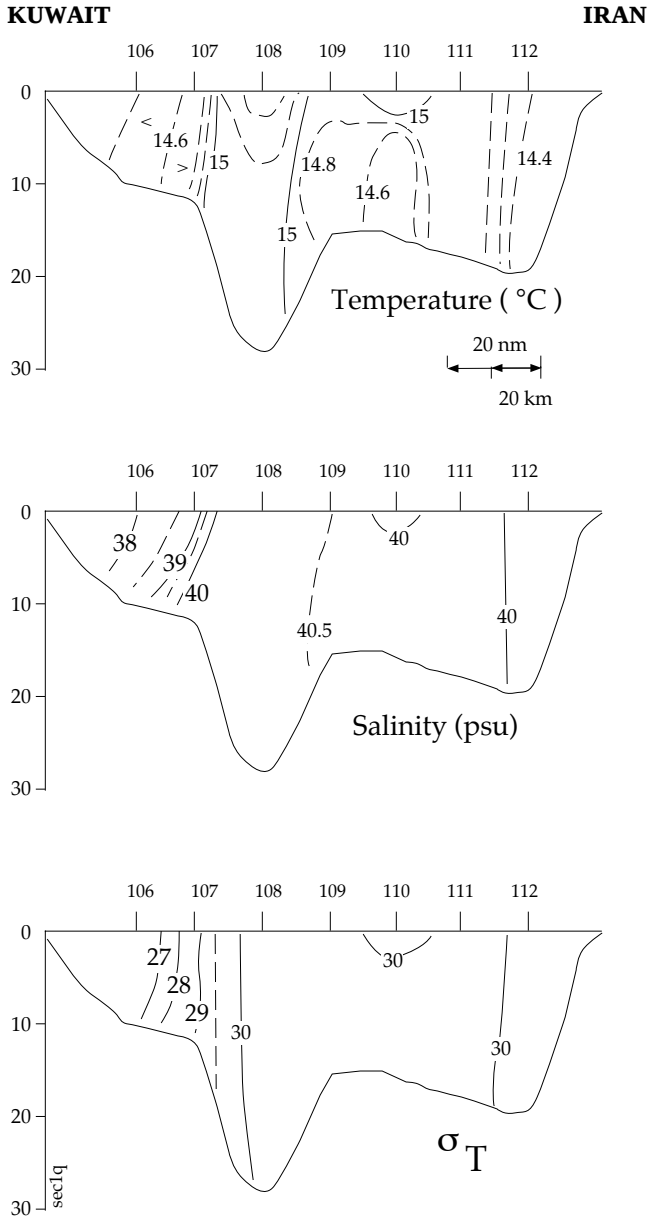

Figure 17: CTD cross section at the northern end of the Persian Gulf along line Q during Leg I (winter)

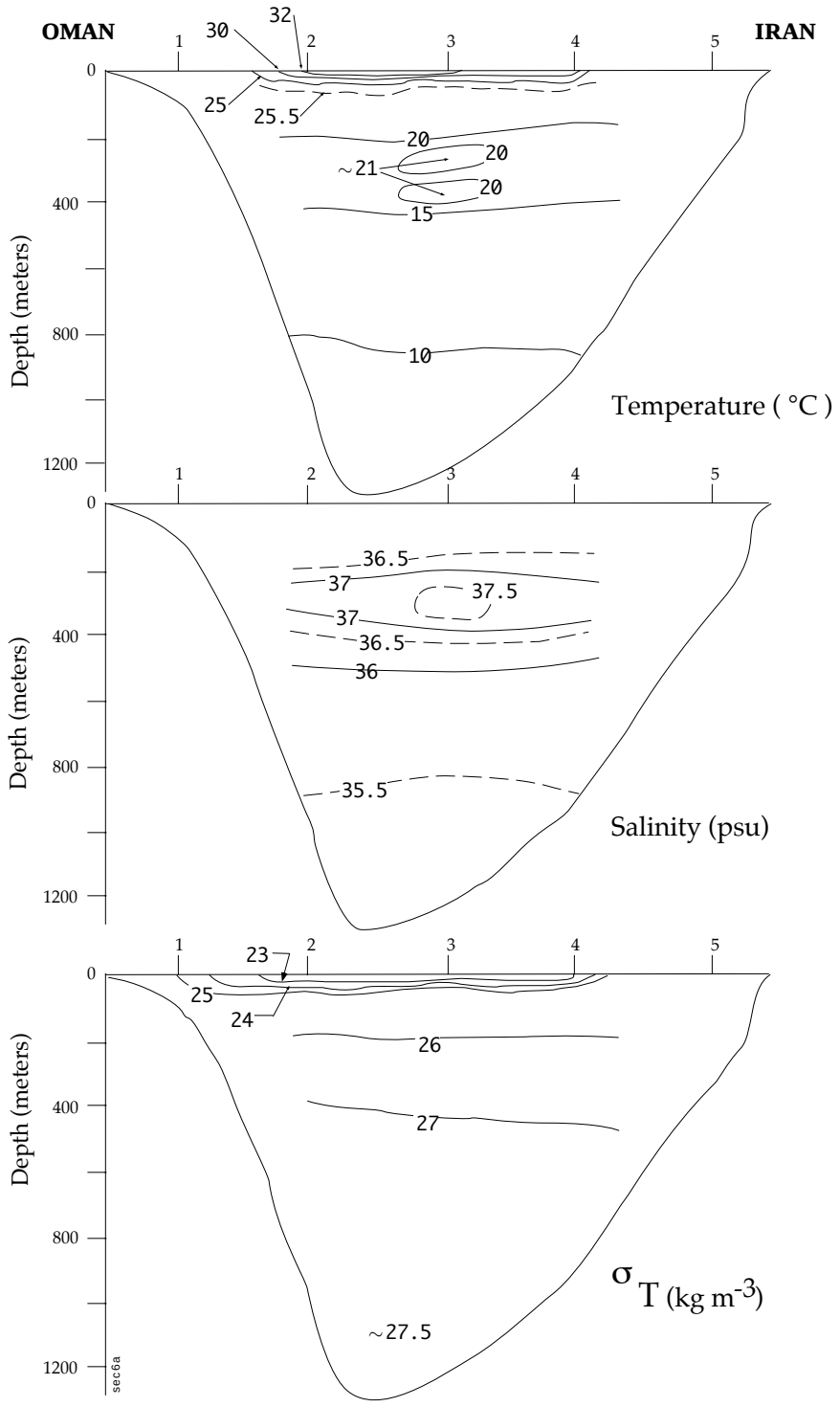

Figure 18: CTD cross section across the Gulf of Oman, along line A, in the Gulf of Oman during Leg VI (summer).

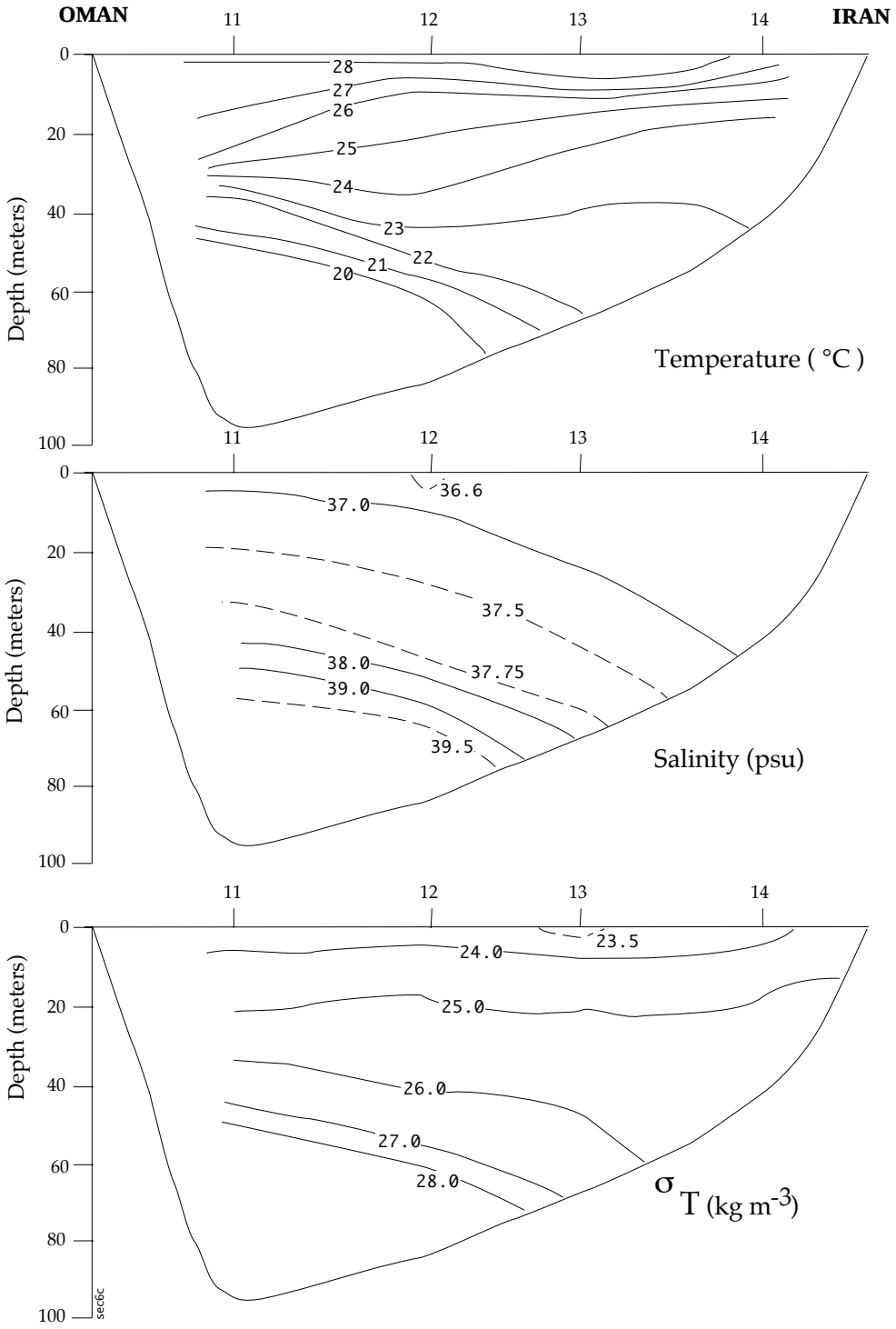

Figure 19: CTD cross section across the Strait of Hormuz, along line C, during Leg VI (summer).

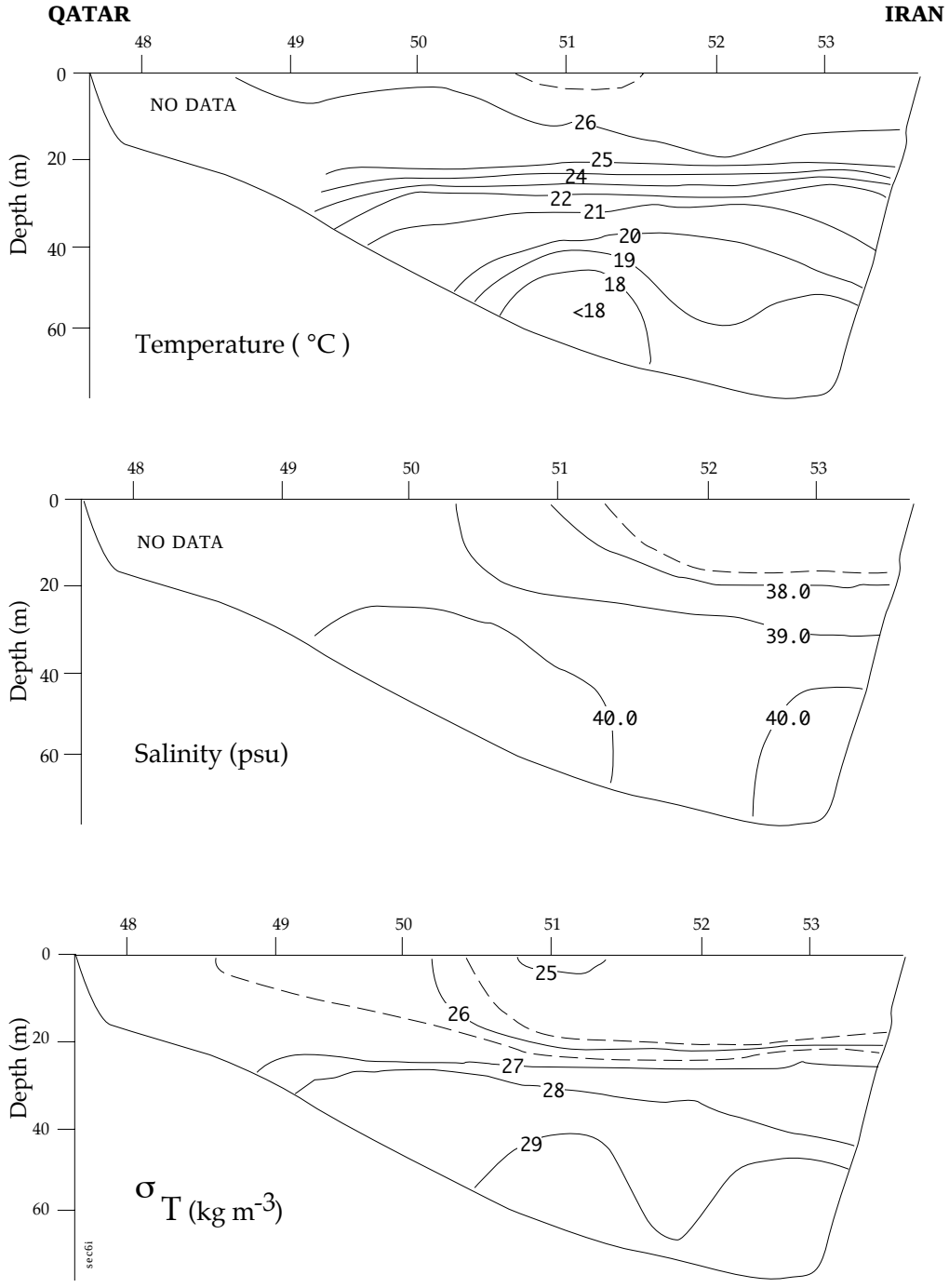

Figure 20: CTD cross section across the central Persian Gulf, along line I, during Leg VI (summer).

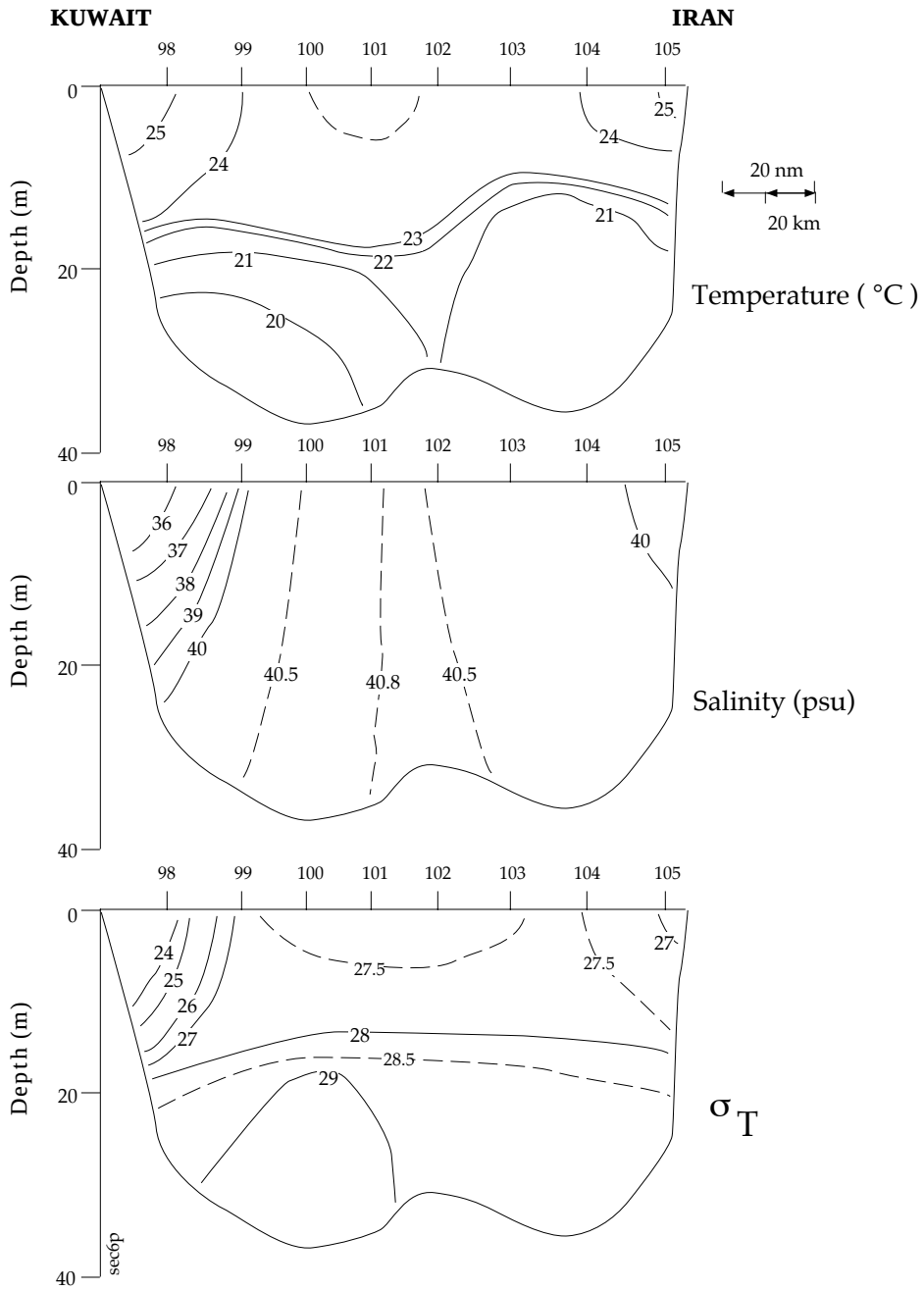

Figure 21: CTD cross section across the north-central Persian Gulf, along line P, during Leg VI (summer).

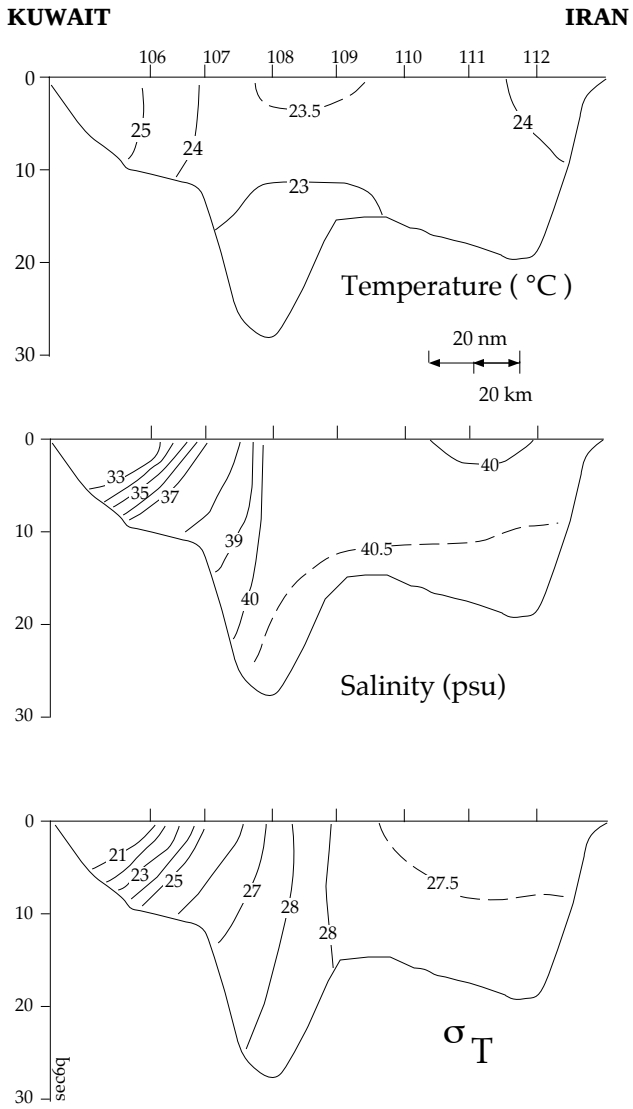

Figure 22: CTD cross section across the northern end of the gulf, along line Q, during Leg VI (summer).

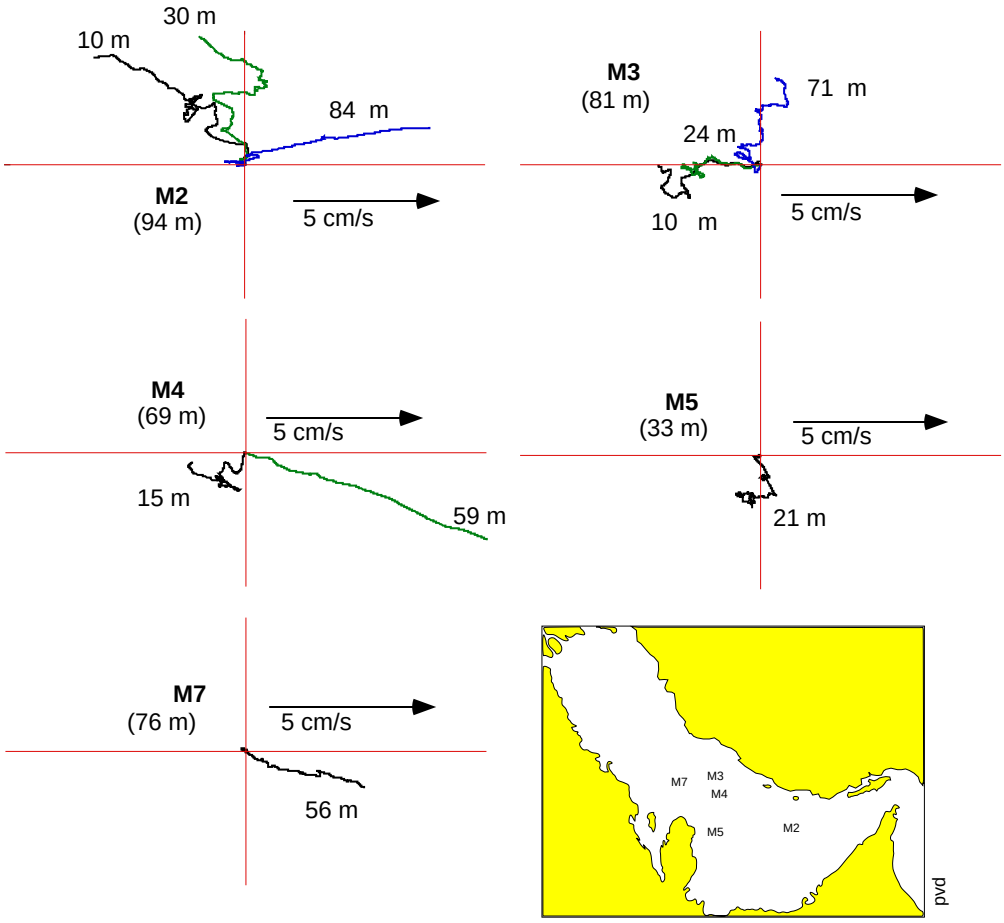

Figure 23: Progressive vector diagrams for filtered current meter records. The upper meters indicate flow towards the NW while bottom meters show return flow towards the Strait of Hormuz. The bottom meter at M3 is suspicious.

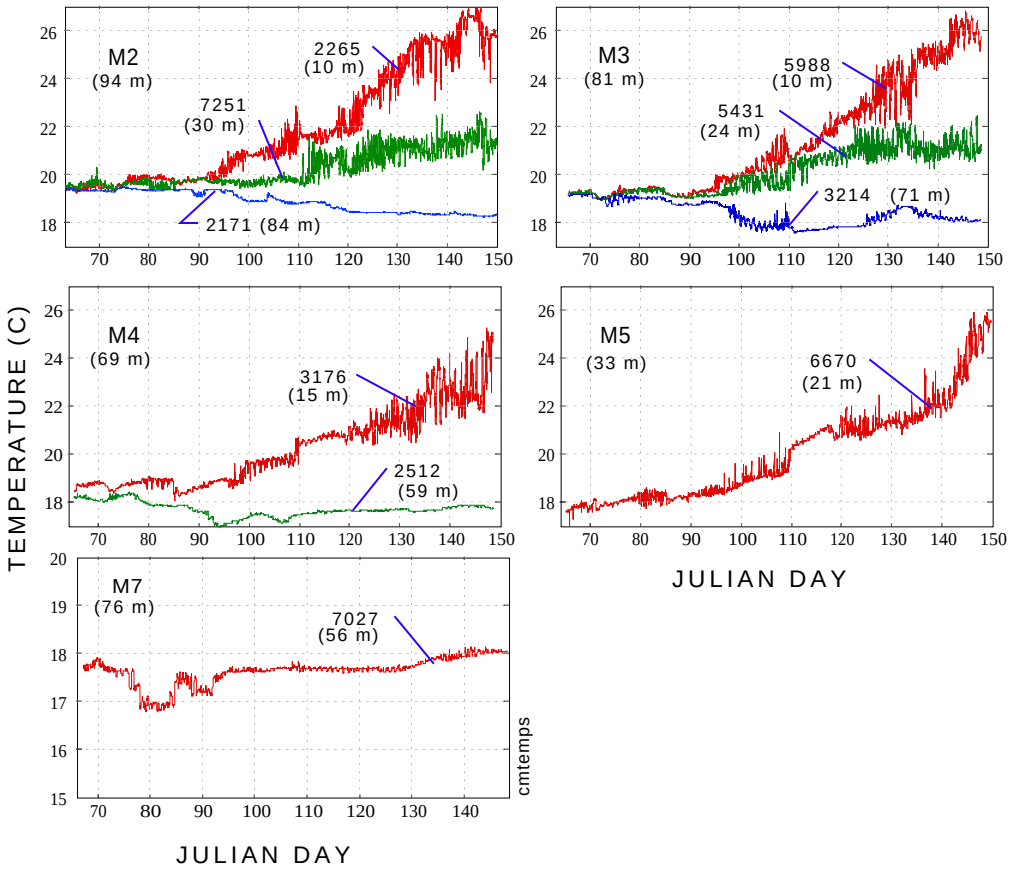

Figure 24: Unfiltered (raw) temperature time series measured by the current meters.

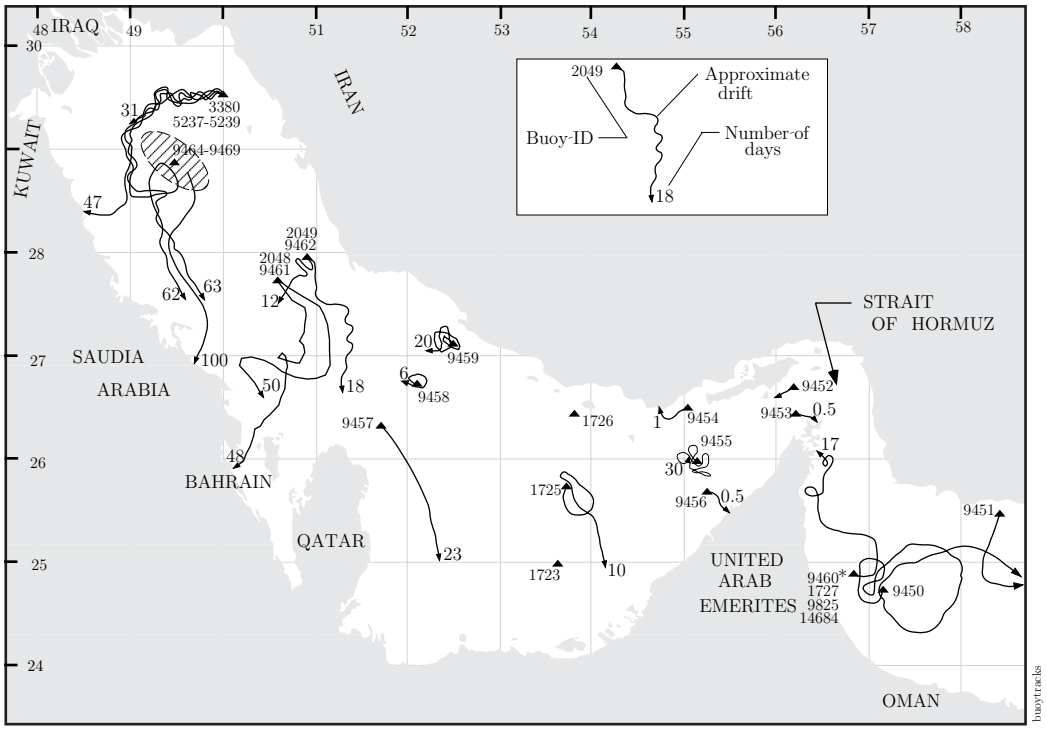

Figure 25: Schematic of the tracks of the drifter buoys. The end of the tracks are marked by an arrow and the number of days of valid data. Buoys 9450 and 9451 drifted out to the Arabian Sea. Buoys 9464–9469 remained in the same location for almost three months until, finally, one buoy drifted away and landed ashore south of Abu Ali Peninsula.

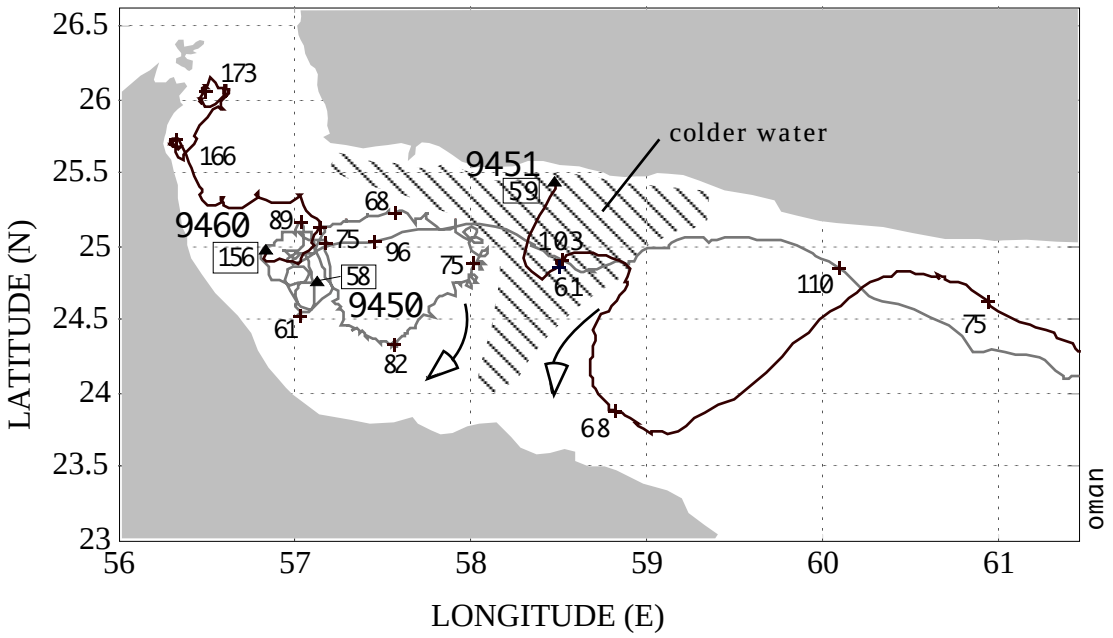

Figure 26: Buoys 9450, 9451, and 9460 indicate a double gyre circulation in the Gulf of Oman. A clockwise circulation in the western provides surface water along the Oman coast and into the Strait of Hormuz. A counter-clockwise circulation exists in the central region. The junction of the two gyres creates a cold water filiment (hatched area) that is evident in satellite sea surface temperature images. Boxed numbers mark the deployment days. Other numbers along the tracks mark the position of the buoys on subsequent Sundays.

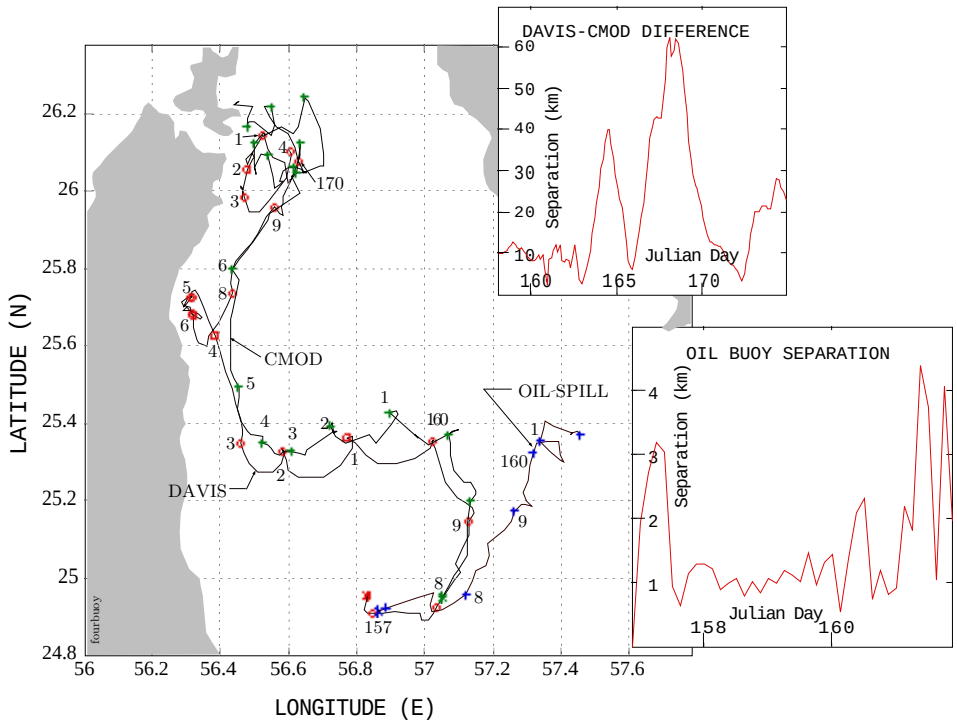

Figure 27: Comparison tracklines of four types of buoys released at the same time in the Gulf of Oman. Tick marks mark the days and the associated number identifies the Julian day for that mark. Top inset shows the separation distance of the Davis and CMOD buoys over a 16-day period. Bottom inset charts separation of the two oil spill buoys during their four-day lifetime.

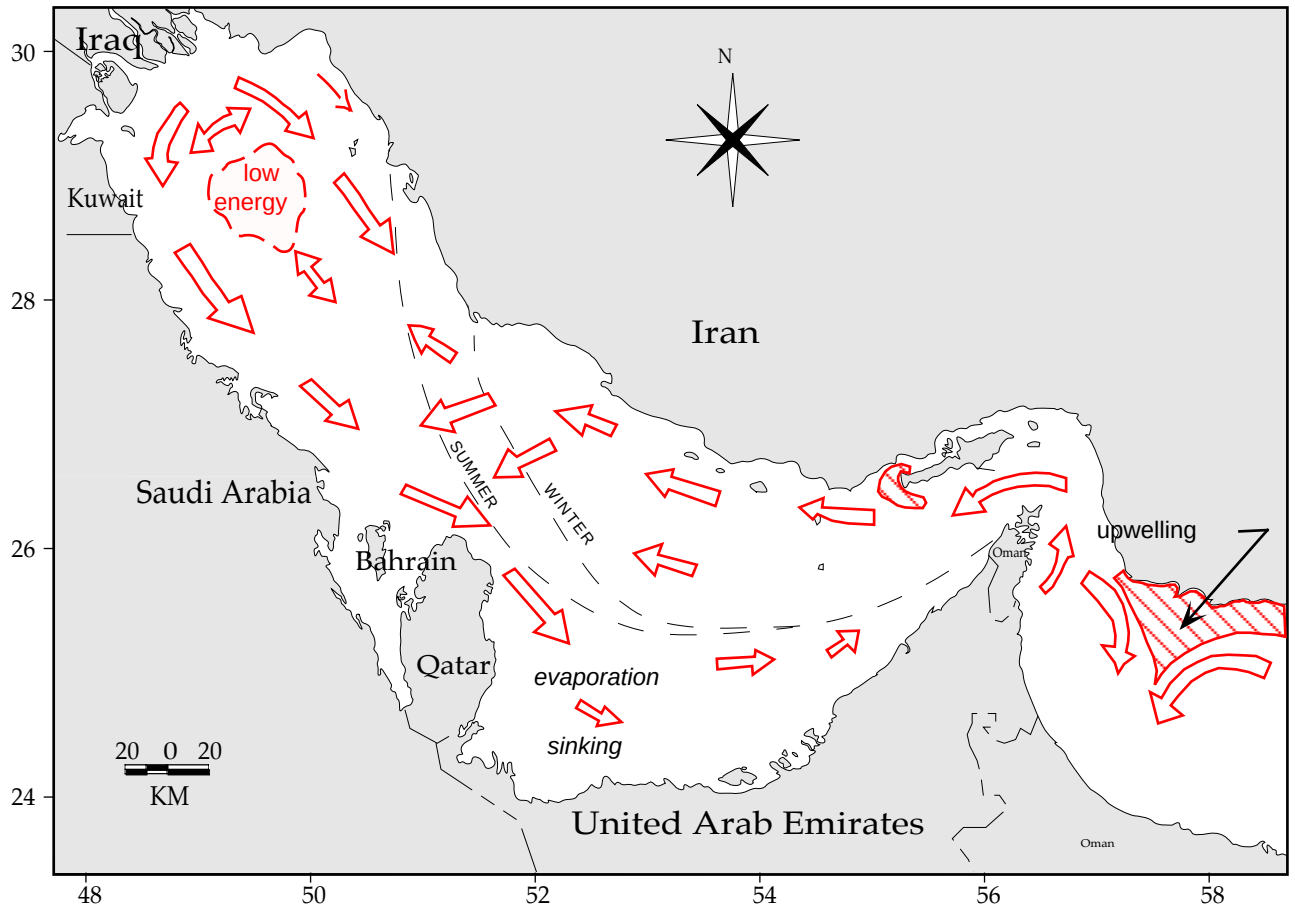

Figure 28: Schematic of surface currents and circulation processes.